Journal of Materials Chemistry A

ROYAL SOCIETY OF CHEMISTRY

PAPER

View Article Online
View Journal | View Issue

Cite this: J. Mater. Chem. A, 2020, 8, 17106

A multifunctional double walled zirconium metal–organic framework: high performance for CO_2 adsorption and separation and detecting explosives in the aqueous phase†

Xiaodong Sun, [ac] Xu Li, [b] Shuo Yao,[a] Rajamani Krishna, [d] Jiaming Gu,[a] Guanghua Li[a] and Yunling Liu *[a]

A rare double walled zirconium metal–organic framework, $[Zr_6O_4(OH)_4(DCPB)_6]\cdot 2DMF\cdot 1H_2O$ (**JLU-Liu45**, 1,3-di(4-carboxyphenyl)benzene (H_2DCPB)), was successfully constructed. Because of its high connectivity, double wall and interpenetration of the framework, **JLU-Liu45** displays extraordinary chemical stability, and is able to maintain an intact framework after being immersed in acid or base solutions. Such a Zr-MOF is also a multifunctional material, which exhibits good capabilities for both CO_2 adsorption and separation and explosives detection in the aqueous phase. Due to the multiple weak C–H···O interactions and narrow pores of the framework, **JLU-Liu45** displays brilliant CO_2 adsorption (116 $cm^3\ g^{-1}$, 1 bar and 273 K) and separation ability (CO_2/N_2 = 81.4, 1 bar and 298 K), surpassing that of state-of-the-art Zr-MOFs reported to date. Additionally, **JLU-Liu45** shows high performance in detecting explosives in the aqueous phase, in which the K_{SV} value towards TNP can reach up to the $10^5\ M^{-1}$ level.

Received 8th May 2020
Accepted 13th July 2020

DOI: 10.1039/d0ta04778c

rsc.li/materials-a

Introduction

Zirconium metal–organic frameworks (Zr-MOFs), which have diverse structure topology, permanent porosity and tunable pore size, have received tremendous attention from both academia and industry since the discovery of the first Zr-MOF (UiO-66) in 2008.[1] The high connectivity and strong Zr–O coordination bonds endow Zr-MOFs with high stability, which can overcome the drawbacks of traditional MOF materials.[2–4] The exceptional stability of Zr-MOFs results in them being considered one of the most promising candidates for application in the field of catalysis, molecular recognition, water harvesting, gas adsorption and separation.[5–10] However, Zr-MOFs with multi-function applications have rarely been reported.

Although Zr-MOFs possess lots of advantages, the number of reported novel Zr-MOFs is relatively small, compared with other metal based MOFs. Because the charge density of Zr(IV) is high, which is not beneficial for ligand exchange during the crystallization process, single crystal growth and structure analysis become difficult.[5,11] Among the reported Zr-MOFs, combining Zr_6 clusters and dicarboxylate ligands usually gives rise to a framework with **fcu**, **bct**, **bcu** and **reo** topologies and a single wall.[1,12–14] However, Zr-MOFs with multiple walls and **pcu** topology have rarely been reported.[15,16] These sorts of Zr-MOFs are provided with many advantages: (1) owing to the increasing of wall thickness, the stability of Zr-MOFs can be further improved; (2) due to the presence of multiple walls, the topology is unpredictable which can contribute to enriching the topology structure of Zr-MOFs; (3) multiple walls of the framework can generate multiple weak interactions between ligands. Such interactions can significantly improve the performance of Zr-MOFs in chemical sensing, gas adsorption and separation.[17–22] In previous work, people often select linear linkers to synthesize Zr-MOFs, but it is difficult to construct multi-walled frameworks.[17,18] In contrast, the V-shaped ligands have more coordination models and spatial adaptabilities which may contribute to constructing Zr-MOFs with multiple walls.

Inspired by the above facts, we utilized the V-shaped ligand and Zr_6 clusters to successfully construct a Zr-MOF $[Zr_6O_4(OH)_4(DCPB)_6]\cdot 2DMF\cdot 1H_2O$ (**JLU-Liu45**, DMF = *N*,*N*-dimethylformamide, H_2DCPB = 1,3-di(4-carboxyphenyl)benzene), which exhibits an interpenetrated 3D framework with unusual

[a]State Key Laboratory of Inorganic Synthesis and Preparative Chemistry, College of Chemistry, Jilin University, Changchun 130012, P. R. China. E-mail: yunling@jlu.edu.cn; Fax: +86-431-85168624; Tel: +86-431-85168614

[b]School of Chemical Engineering and Light Industry, Guangdong University of Technology, Guangzhou 510006, Guangdong, P. R. China

[c]Institute of Clean Energy Chemistry, Key Laboratory for Green Synthesis and Preparative Chemistry of Advanved Materials, College of Chemistry, Liaoning University, Shenyang 110036, China

[d]Van't Hoff Institute for Molecular Sciences, University of Amsterdam, Science Park 904, 1098 XH Amsterdam, The Netherlands

† Electronic supplementary information (ESI) available: Structure information, XRD, TGA, and isosteric heat of CH_4, C_2H_6 and C_3H_8. Crystal data and structure refinement. CCDC 1557570. For ESI and crystallographic data in CIF or other electronic format see DOI: 10.1039/d0ta04778c

double walls. Because of multiple walls and interpenetration of the framework, **JLU-Liu45** possesses extraordinary thermal and chemical stability. **JLU-Liu45** is also a multifunctional material, which exhibits good capabilities for both CO_2 adsorption and separation and explosives detection in the aqueous phase. Although its BET surface area is not prominent, lower than that of majority of Zr-MOFs,[23–25] its CO_2 uptake value is impressive, which is as high as 116 $cm^3\ g^{-1}$ at 273 K. The selectivity of **JLU-Liu45** for CO_2/N_2 exceeds that of state-of-the-art Zr-MOFs reported to date. Moreover, it also exhibits high performance for detecting explosives in the aqueous phase, in which the K_{SV} value for monitoring 2,4,6-trinitrophenol (TNP) is 2.3×10^5 M^{-1}, which exceeds those of most of the reported water stable MOFs and other types of materials.

Experimental

Safety precautions

Caution! TNP is highly explosive and should be handled carefully and in small amounts. The explosives were handled as dilute solutions using safety measures to avoid explosion.

General information

All the chemicals were of analytical grade and used without further purification. C, H, and N elemental analyses were achieved on a Vario MICRO instrument (Elementar, Germany). A Rigaku D/max-2550 diffractometer with Cu-Kα radiation (λ = 1.5418 Å) was employed to collect Powder X-ray Diffraction (PXRD) data (4–40°) at ambient temperature. Fluorescence spectra were collected on a Fluoromax-4 spectrophotometer at ambient temperature with a slit width and filter of 2 nm and 360 nm, respectively. A TGA Q500 thermogravimetric analyzer was used to perform the thermal gravimetric analyses (TGA) with a heating rate of 10 °C min^{-1} in air.

Preparation of JLU-Liu45

Colorless rod like crystals of **JLU-Liu45** were synthesized *via* a solvothermal reaction of H_2DCPB (15 mg, 0.05 mmol), $ZrCl_4$ (13 mg, 0.05 mmol), DMF (2.0 mL) and acetic acid (0.25 mL, 0.004 mmol) at 115 °C for 48 h (yield 85%, based on H_2DCPB). Through comparing the experimental PXRD patterns and simulated patterns derived from single crystal X-ray diffraction, the purity of **JLU-Liu45** was verified (Fig. S1†).

X-ray crystallography

A Bruker Apex II CCD diffractometer instrument was employed to collect **JLU-Liu45** crystallographic data at ambient temperature. Through direct methods and refined by full-matrix least-squares on F^2 using version 5.1, the structure of **JLU-Liu45** could be solved.[26] Firstly, all the metal atoms were located. Secondly, the O and C atoms of the **JLU-Liu45** were determined in the difference Fourier maps. Thirdly, the H atoms of H_2DCPB were determined geometrically. All non-hydrogen atoms were refined anisotropically. Finally, the final formula of **JLU-Liu45** was defined by combining the crystallographic data and elemental and thermogravimetric analysis data. Tables S1 and S2† present the crystal data and structure refinement, selected bond lengths and angles of **JLU-Liu45**. Crystallographic data for **JLU-Liu45** (1557570) have been deposited. Based on TOPOS 4.0, the topology information of **JLU-Liu45** was also calculated.[27]

Gas adsorption measurements

N_2 gas adsorption measurements were carried out Micromeritics ASAP 2420, and CO_2 and small alkane gas measurements were performed on Micromeritics 3-Flex. Before gas adsorption measurements, the nonvolatile solvent molecules in the MOF should be removed, thus achieving full activation. Then, the samples were dried under dynamic vacuum at 30 °C for 2 hours. Lastly, the samples were dried again through utilizing the 'outgas' function of the Micromeritics analyzer for 1 h at 30 °C and then 9 h at 100 °C.

Computational simulation studies of CO_2 adsorption

Based on the Grand Canonical Monte Carlo (GCMC) simulation, the density distribution of CO_2 molecules was calculated at 298 K and 1 bar. The Universal Force Field (UFF) and periodic boundary conditions were also employed.[28] Then, the electrostatic interaction in the Zr-MOF was evaluated through the Ewald summation method. Through utilizing Lennard-Jones potentials, van der Waals interactions between CO_2 and Zr-MOF were also calculated. The cutoff distance was set at 18.5 Å. The atom charges of the CO_2 molecule and the Zr-MOF structure were obtained from the density functional theory (DFT) calculations. The generalized gradient approximation (GGA) of the Perdew–Burke–Ernzerhof (PBE) method was executed to treat the exchange and correlation potentials.[29] The double numerical basis set (DND basis set) was also employed. All the GCMC simulations and DFT calculations were performed utilizing the Material Studio software of Sorption and Dmol^3 modules, respectively.

Luminescence sensing experiments

The solid-state luminescent properties of H_2DCPB ligands and MOF samples were tested at ambient temperature. H_2DCPB ligand displays fluorescent emissions at 380 nm upon excitation at 323 nm (Fig. S18†). Compared with the free ligand, **JLU-Liu45** exhibits a similar emission at 388 nm under the excitation at 323 nm. Albeit a blue-shift of 8 nm is observed between the ligand and the crystal, the result also indicates that the fluorescent property of **JLU-Liu45** is mostly because of the organic linkers. Furthermore, the samples of **JLU-Liu45** were dispersed in various solvents, such as DMF, *N*,*N*′-dimethylacetamide (DMA), dioxane, acetonitrile, acetone, ethanol and water, and then their fluorescent properties were further tested. The results clearly demonstrated that the fluorescent emission of **JLU-Liu45** exhibits a large solvent dependence. Although the fluorescence intensity of **JLU-Liu45** was decreased after it was immersed in the solvents of acetone and acetonitrile, it exhibits excellent fluorescence intensity in water (Fig. S19†). Seven organic explosives (nitrobenzene (NB), TNP, methylbenzene (MB), 4-nitrophenol (4-NP), nitromethane (NM), phenol (PHL) and 2,3-

dimethyl-2,3-dinitrobutane (DMNB)) were chosen to assess the ability of **JLU-Liu45** for detecting organic explosives in water.

For the credibility of the experiment, all the sensing tests were carried out in water at ambient temperature. Before measurement, 2 mg **JLU-Liu45** samples are dispersed in 2 mL water. Then fluorescence quenching titrations were carried out through adding the organic explosives (1 mM, 20 μL additions each time) piece by piece. Based on the Stern–Volmer (SV) equation $(I_0/I) = K_{SV}[Q] + 1$, the quenching efficiency was calculated, in which the I_0 and I represent the fluorescence intensities of the samples before and after the sensing tests, and Q and K_{SV} represents the organic explosive concentration and corresponding quenching constant (M^{-1}).[30]

Result and discussion

Structure of JLU-Liu45

According to the single-crystal X-ray diffraction result, **JLU-Liu45** crystallizes in the $R\bar{3}$ space group and exhibits an interpenetrated 3D framework. The V-shaped ligand should be regarded as a linear rod which connects two classical $Zr_6O_4(OH)_4(CO_2)_{12}$ secondary building units (SBUs), while the Zr_6 cluster is coordinated to twelve V-shaped ligands and should be regarded as cuboctahedral geometry (Fig. 1a). Albeit the connectivity of the SBUs is in accordance with the UiO series MOFs,[1,31–34] the single net of the framework shows that the pore walls of **JLU-Liu45** are constructed through one pair of V-shaped ligands (Fig. 1b). Analyzing from the perspective of topology, the whole structure of **JLU-Liu45** should be classified as a framework with **pcu** topology, in virtue of the presence of a double wall (Fig. 1c and S3†). To the best of our knowledge, the combination of Zr_6 clusters and dicarboxylate ligands usually gives rise to **fcu**, **bct**, **bcu** and **reo** topologies with a single wall (Fig. S4†). It has rarely been reported that a porous Zr-MOF constructed from a dicarboxylate ligand and exhibits **pcu** topology with a double wall.[15,16] Although the interpenetration reduces the porosity of the framework, it still possesses one-dimensional triangle channels with a side length of 5 Å, considering van der Waals radius along the *c* axis (Fig. 1d and S5†). Viewing along the *c* axis, two types of helical chains, which are comprised of two nets of the framework with left and right-handed helical directions, can also be observed in the framework of **JLU-Liu45** (Fig. 1d). The structure of **JLU-Liu45** is similar to that of **BUT-66** (ref. 16) which shows excellent capture of trace aromatic volatile organic compounds in ambient air, while **JLU-Liu45** exhibits good capabilities for both CO_2 adsorption/separation and explosive detection in the aqueous phase.

Gas adsorption and separation ability

To confirm the permanent porosity of **JLU-Liu45**, N_2 adsorption measurements were performed at 77 K. They display a fully reversible type-I isotherm characteristic, which indicates that **JLU-Liu45** is a microporous material. The Langmuir and Brunauer–Emmett–Teller (BET) surface areas of **JLU-Liu45** are estimated to be 1101 and 971 $m^2\ g^{-1}$, respectively. Pore size distributions of **JLU-Liu45** were calculated by the DFT method based on the N_2 adsorption isotherm, revealing a distinct peak at 5.5 Å, in full agreement with the crystallographic structure determination considering the van der Waals radius (Fig. S6†).

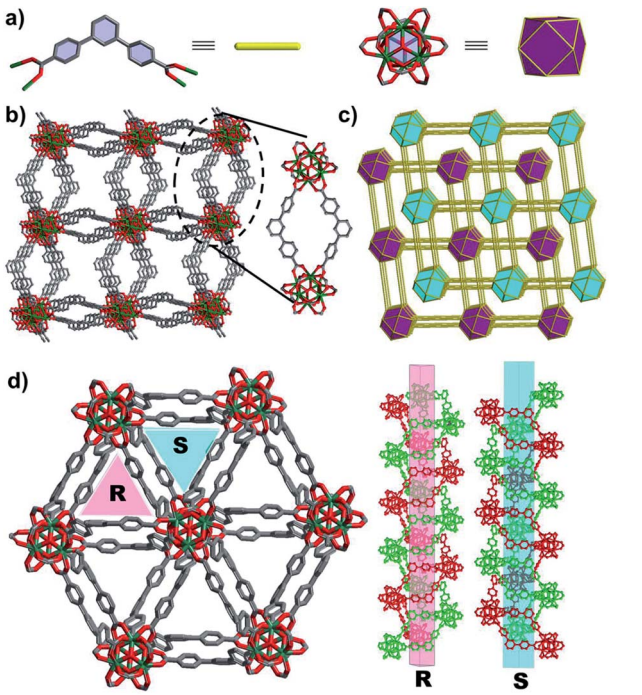

Fig. 1 Structural analysis of **JLU-Liu45**: (a) topology simplification of the H_2DCPB ligand and the 12-connected Zr_6 cluster; (b) double layers of the pore wall and single net of the framework; (c) polyhedral view of the interpenetrated net; (d) helixes with opposite handedness along the *c* axis. C = grey; O = red; Zr = dark green (hydrogen and guest molecules interspersed in the structure are omitted for a succinct packing).

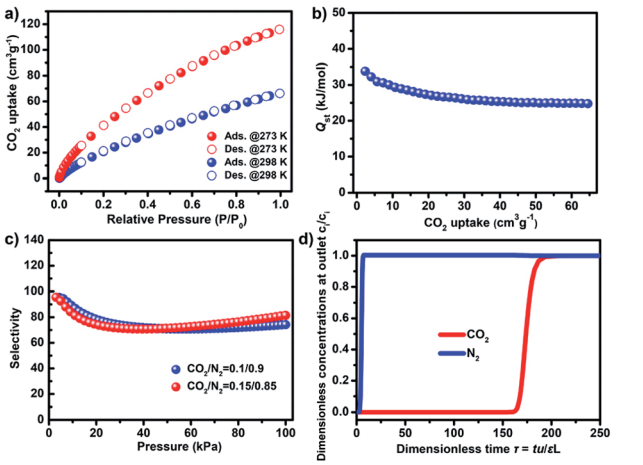

Fig. 2 (a) CO_2 adsorption isotherms of **JLU-Liu45**; (b) Q_{st} of CO_2 for **JLU-Liu45**; (c) based on the IAST method, CO_2/N_2 gas adsorption selectivity for **JLU-Liu45** is predicted at 298 K and 100 kPa; (d) transient breakthrough simulations for separation of the 15/85 CO_2/N_2 mixture in **JLU-Liu45** at 100 kPa and 298 K. The *y*-axis is dimensionless concentrations at the exit, normalized with respect to the inlet concentrations.

In light of the small pores and multiple adsorption sites created by the interpenetration of the framework, **JLU-Liu45** may be considered an excellent candidate for CO_2 adsorption and separation. To corroborate our assumption, the CO_2 adsorption ability of the activated samples was investigated. As depicted in Fig. 2a, **JLU-Liu45** display high capability for CO_2 adsorption, in which its CO_2 adsorption capacities are 116 and 66 $cm^3\ g^{-1}$ at 273 and 298 K (1 bar), respectively. In comparison with other Zr-MOFs, its BET surface area is not prominent, but CO_2 uptake values at 273 and 298 K are impressive, which are comparable to many OMS or LBS decorated Cu-MOFs, such as MAF-35 and rht-MOF-7,[35–37] and surpass many reported Zr-MOFs (Table S6†).[38–43] To further understand CO_2 adsorption properties of **JLU-Liu45**, the isosteric heat (Q_{st}) of adsorption was calculated based on the adsorption isotherms at 273 and 298 K. The Q_{st} value of **JLU-Liu45** is about 34 kJ mol^{-1}, which is higher than those of most reported Zr-MOFs, such as BUT-10, BUT-11 and UiO-67 (Fig. 2b and Table S6†).[38–43] Moreover, some small alkanes were also selected to estimate its gas adsorption properties (Fig. S11–13† and Table S7†).

The excellent CO_2 adsorption ability found in **JLU-Liu45** prompted us to further estimate the practical separation ability of **JLU-Liu45** for CO_2 over CH_4 and N_2. Different gas mixtures of CO_2/CH_4 (0.5/0.5 and 0.05/0.95) and CO_2/N_2 (0.1/0.9 and 0.15/0.85) were theoretically calculated by the ideal adsorbed solution theory (IAST) model. By using the dual-site Langmuir–Freundlich equation, the model fits the adsorption isotherm at 298 K very well ($R^2 > 0.9999$) (Fig. S14a and c†).[44–46] The fitting parameters are used to predict multicomponent adsorption with IAST. The selectivity values of **JLU-Liu45** for CO_2 over CH_4 are 7.0 and 8.2 at 298 K and 1 bar (Fig. S14b†), which surpass many MOFs with high ability for the separation of CO_2 over CH_4 under the same conditions (Table S9†).[47–50]

Importantly, the selectivity values for CO_2 over N_2 are 74.2 and 81.4 (Fig. 2c), surpassing those of state-of-the-art Zr-MOFs reported to date and much higher than those of most stable MOFs (Table S8†).[51–55] Additionally, its separation performance for the industrially important small hydrocarbons were also calculated by the method of IAST (Fig. S15†).

According to the reported literature, transient breakthrough simulations were performed using the simulation methodology to further evaluate the separation performance of **JLU-Liu45** for CO_2 over CH_4 and N_2.[56,57] We investigated the transient breakthrough simulations for separation of (50/50 and 5/95) CO_2/CH_4 and (15/85 and 10/90) CO_2/N_2 mixtures in a fixed bed packed with **JLU-Liu45** operating at 298 K under 1 bar. Typically, the longer the CO_2 molecules remain trapped within the bed, the more efficient the gas separation is. As shown in Fig. 2d and S16,† the breakthrough time is 122 and 158 for CO_2/CH_4, and 165 and 175 for CO_2/N_2, respectively. The values are excellent among the simulated MOFs, so the breakthrough results also indicate that **JLU-Liu45** is suitable for the selectivity of CO_2.

To explain the remarkable CO_2 capture and the commendable isosteric heat value, Grand Canonical Monte Carlo (GCMC) simulations were carried out to investigate the interactions between CO_2 molecules and activated **JLU-Liu45** by using the sorption module of Materials Studio.[28,29] The simulated

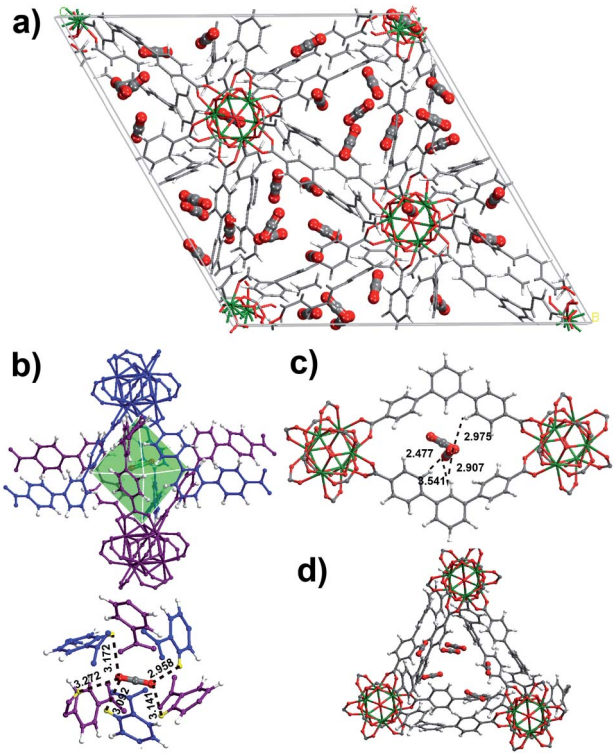

Fig. 3 (a) Simulation snapshot for CO_2 molecules in the JLU-Liu45 framework. Three CO_2 binding sites and the closed binding distances were analyzed from the snapshot: (b) inside the cage; (c) on the top of the Zr center; (d) in the triangle channel of the JLU-Liu45 framework.

adsorption amount for **JLU-Liu45** at 298 K under 1 bar is 22 CO_2 per cage, which is close to the experimental value (23 CO_2 per cage). The preferential CO_2 adsorption sites given by the simulation are shown in Fig. 3a. The high CO_2 capture and the commendable isosteric heat value can be ascribed to the following reasons: (1) the CO_2 molecule can locate in the small cage of the framework formed by two interpenetrated nets of **JLU-Liu45**, in which the multiple weak C–H···O interactions between the CO_2 molecule and H_2DCPB ligands with short H···O distances of 2.958–3.272 Å enhance the CO_2 adsorption ability (Fig. 3b); (2) the double wall in the framework of **JLU-Liu45** could form small pockets which are suitable for the adsorption of CO_2 molecules. As depicted in Fig. 3c, the short C–H···O distances of 2.477, 2.907 and 2.975 Å in such pockets promote the assembly of the multiple weak C–H···O interactions between the CO_2 molecule and the H_2DCPB ligand; (3) in spite of the interpenetration reducing the pore dimensions, the triangle pore size is suitable for the CO_2 molecule (Fig. 3d). Meanwhile, more adsorption sites could be created by the framework interpenetration. Therefore, the GCMC result indicates that the high CO_2 adsorption capacity and Q_{st} values are due to the multiple host-guest C–H···O interactions and the narrow pores formed by the interpenetration of the framework.

Luminescence sensing of explosives in the aqueous phase

Although many MOFs have been explored for detecting explosives since the first example was reported by Li *et al.*,[58] most of

them are limited in use because of their poor water stability. Benefitting from the excellent water stability and non-toxic Zr(IV) metal centers, **JLU-Liu45** may be a good candidate for monitoring the target nitro explosives in the aqueous phase. Inspired by the above facts, we attempted to explore the fluorescent sensing properties of **JLU-Liu45** to detect a series of nitro explosives, including NB, TNP and 4-NP. For comparison, a series of aromatics and aliphatic organic explosives such as NM, PHL, MB and DMNB were also tested. As shown in Fig. 4a and c, **JLU-Liu45** exhibits fast and high fluorescence quenching efficiencies after the addition of 20 μL 1 mM TNP and 4-NP aqueous solutions. Fluorescence quenching can also be clearly observed for NB, but the other aliphatic nitro and non-nitroaromatics compounds exert minor effects on the fluorescence intensity of **JLU-Liu45** (Fig. S20–24†). The quenching efficiencies of **JLU-Liu45** follow the sequence of TNP > 4-NP > NB > PHL > DMNB > NM > MB (Fig. S24†). To illustrate the fluorescence quenching mechanism of **JLU-Liu45**, its electron transfer mechanism was calculated by DFT calculation. According to previous reports, MOFs are a kind of large molecule, in which the valence and conduction-band energy levels can be represented by the molecular orbital mode.[38] When the lowest unoccupied molecular orbital (LUMO) of the analyte is lower than the conduction-band energy of MOFs, the electrons will transfer from the MOFs to the analyte, thus leading to fluorescence quenching. With a lower LUMO of the analyte, the electrons will more easily transfer from MOFs to the analyte. As illustrated in Fig. S33,† the LUMO energy of TNP is the lowest among all selected organic explosives. Therefore, the electrons of **JLU-Liu45** can easily transfer to TNP, thus giving the highest quenching efficiency. However, the quenching efficiency of other organic explosives is not in accordance with the LUMO energies, which suggests that electron transfer is not the only reason for the quenching efficiency. Then, the energy transfer mechanism was also investigated. As depicted in Fig. S34,† the overlapping between the emission spectrum of **JLU-Liu45** and the absorption spectrum of TNP is the largest among all selected organic explosives. Therefore, the energy can be easily transferred from **JLU-Liu45** to TNP, thus resulting in the highest quenching efficiency. The overlapping proportion between the emission spectrum of **JLU-Liu45** and the absorption spectra of organic explosives follows the sequence of TNP, 4-NP, NB, PHL, DMNB, NM, and MB, which is in accordance with their quenching efficiency. Based on the above results, the excellent quenching efficiency of **JLU-Liu45** for detecting TNP can be ascribed to a synergistic effect of electron transfer and energy transfer. After five cycles of repeated fluorescent measurements, the fluorescence intensity and the PXRD patterns of the materials exhibit little change which further indicates its excellent recyclability (Fig. S26 and S27†). As depicted in Fig. 4b and d, the SV plots for detecting TNP and 4-NP are nearly linear initially, while on further increasing the concentration, the plots latterly deviate from linearity, which can be attributed to the self-absorption effect.[15] On the other hand, the other aliphatic nitro and non-nitroaromatic compounds produce a linear plot (Fig. S20–24†). It is commendable that the K_{SV} value of **JLU-Liu45** for detecting TNP is about 2.3×10^5 M^{-1}, which exceeds those of many reported water stable MOFs (Table S10†).[59–63] Then the selectivity of **JLU-Liu45** towards TNP and 4-NP was further studied (Fig. S28–32†). The results demonstrate that even in the presence of other aliphatic nitro and non-nitroaromatic compounds, **JLU-Liu45** exhibits outstanding selectivity towards 4-NP and TNP.

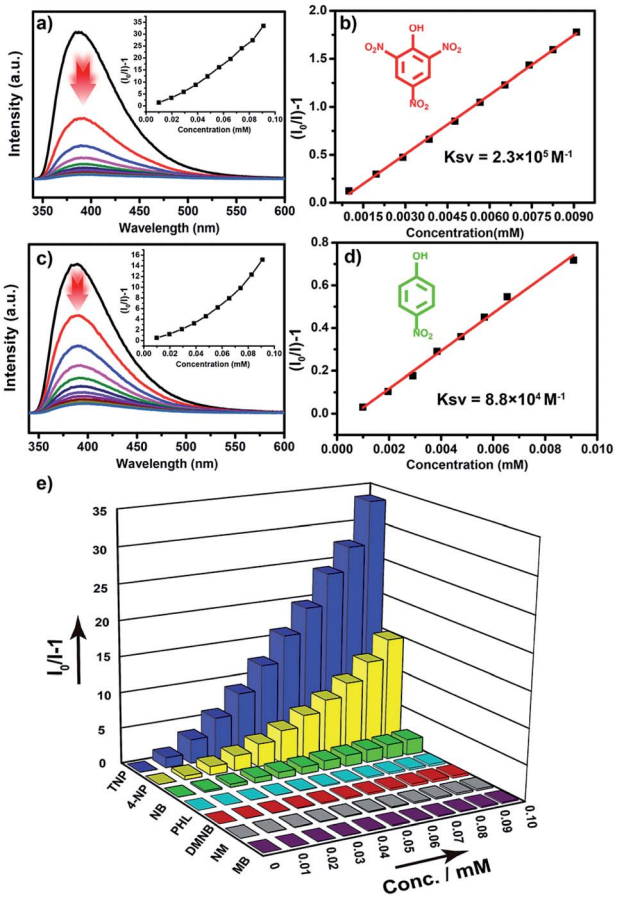

Fig. 4 The emission spectra for **JLU-Liu45** after titration with TNP (a) and 4-NP (c) in H_2O for 1 minute, respectively (1 mM, 20 μL addition each time); inset images represent the SV plots of corresponding organic explosives. The SV plots for **JLU-Liu45** with TNP (b) and 4-NP (d) in the low concentration region. (e) Stern–Volmer plots of selected nitroaromatics and non-nitroaromatics in **JLU-Liu45**.

Conclusion

In summary, the judicious choice of V-shape ligand results in an interpenetrated Zr-MOF (**JLU-Liu45**) that not only possesses double walls but also displays extraordinary thermal and chemical stability. Benefitting from the small pores and adsorption sites which are the result of interpenetration, **JLU-Liu45** exhibits brilliant CO_2 adsorption and separation ability. On the other hand, it also exhibits high performance for detecting TNP in the aqueous phase. Consequently, **JLU-Liu45** is a multifunctional Zr-MOF, which is potentially useful in monitoring water quality along with CO_2 capture and separation. The groundbreaking preparation of double walled Zr-

MOFs affords new directions for the construction of novel Zr-MOFs.

Conflicts of interest

There are no conflicts to declare.

Acknowledgements

This work was financially supported by the National Natural Science Foundation of China (No. 21771078 and 21621001), the 111 Project (B17020), and the National Key Research and Development Program of China (2016YFB0701100).

Notes and references

1 J. H. Cavka, S. Jakobsen, U. Olsbye, N. Guillou, C. Lamberti, S. Bordiga and K. P. Lillerud, *J. Am. Chem. Soc.*, 2008, **130**, 13850–13851.
2 J. Canivet, A. Fateeva, Y. Guo, B. Coasne and D. Farrusseng, *Chem. Soc. Rev.*, 2014, **43**, 5594–5617.
3 N. C. Burtch, H. Jasuja and K. S. Walton, *Chem. Rev.*, 2014, **114**, 10575–10612.
4 J. B. Decoste, G. W. Peterson, M. W. Smith, C. A. Stone and C. R. Willis, *J. Am. Chem. Soc.*, 2012, **134**, 1486–1489.
5 Y. Bai, Y. Dou, L. H. Xie, W. Rutledge, J. R. Li and H. C. Zhou, *Chem. Soc. Rev.*, 2016, **45**, 2327–2367.
6 W. Gong, X. Chen, H. Jiang, D. Chu, Y. Cui and Y. Liu, *J. Am. Chem. Soc.*, 2019, **141**, 7498–7508.
7 A. Mallick, A. M. El-Zohry, O. Shekhah, J. Yin, J. Jia, H. Aggarwal, A.-H. Emwas, O. F. Mohammed and M. Eddaoudi, *J. Am. Chem. Soc.*, 2019, **141**, 7245–7249.
8 S. Wang, N. Xhaferaj, M. Wahiduzzaman, K. Oyekan, X. Li, K. Wei, B. Zheng, A. Tissot, J. Marrot, W. Shepard, C. Martineau-Corcos, Y. Filinchuk, K. Tan, G. Maurin and C. Serre, *J. Am. Chem. Soc.*, 2019, **141**, 17207–17216.
9 R. G. AbdulHalim, P. M. Bhatt, Y. Belmabkhout, A. Shkurenko, K. Adil, L. J. Barbour and M. Eddaoudi, *J. Am. Chem. Soc.*, 2017, **139**, 10715–10722.
10 E.-X. Chen, M. Qiu, Y.-F. Zhang, Y.-S. Zhu, L.-Y. Liu, Y.-Y. Sun, X. Bu, J. Zhang and Q. Lin, *Adv. Mater.*, 2018, **30**, 1704388.
11 Q. Lin, X. Bu, A. Kong, C. Mao, X. Zhao, F. Bu and P. Feng, *J. Am. Chem. Soc.*, 2015, **137**, 2235–2238.
12 H. Furukawa, F. Gándara, Y.-B. Zhang, J. Jiang, W. L. Queen, M. R. Hudson and O. M. Yaghi, *J. Am. Chem. Soc.*, 2014, **136**, 4369–4381.
13 V. Bon, V. Senkovskyy, I. Senkovska and S. Kaskel, *Chem. Commun.*, 2012, **48**, 8407–8409.
14 S. Yuan, W. Lu, Y. P. Chen, Q. Zhang, T. F. Liu, D. Feng, X. Wang, J. Qin and H. C. Zhou, *J. Am. Chem. Soc.*, 2015, **137**, 3177–3180.
15 X. Sun, S. Yao, C. Yu, G. Li, C. Liu, Q. Huo and Y. Liu, *J. Mater. Chem. A*, 2018, **6**, 6363–6369.
16 L.-H. Xie, X.-M. Liu, T. He and J.-R. Li, *Chem*, 2018, **4**, 1911–1927.
17 D. Tian, Q. Chen, Y. Li, Y. H. Zhang, Z. Chang and X. H. Bu, *Angew. Chem., Int. Ed.*, 2014, **53**, 837–841.
18 D. Tian, J. Xu, Z. J. Xie, Z. Q. Yao, D. L. Fu, Z. Zhou and X. H. Bu, *Adv. Sci.*, 2016, **3**, 1500283.
19 J. An, O. K. Farha, J. T. Hupp, E. Pohl, J. I. Yeh and N. L. Rosi, *Nat. Commun.*, 2012, **3**, 604.
20 X. Lin, I. Telepeni, A. J. Blake, A. Dailly, C. M. Brown, J. M. Simmons, M. Zoppi, G. S. Walker, K. M. Thomas, T. J. Mays, P. Hubberstey, N. R. Champness and M. Schröder, *J. Am. Chem. Soc.*, 2009, **131**, 2159–2171.
21 A. Schaate, P. Roy, T. Preuße, J. Lohmeier Sven, A. Godt and P. Behrens, *Chem.–Eur. J.*, 2011, **17**, 9320–9325.
22 Y. K. Park, S. B. Choi, H. Kim, K. Kim, B. H. Won, K. Choi, J. S. Choi, W.-S. Ahn, N. Won, S. Kim, D. H. Jung, S. H. Choi, G. H. Kim, S. S. Cha, Y. H. Jhon, J. K. Yang and J. Kim, *Angew. Chem., Int. Ed.*, 2007, **119**, 8378–8381.
23 T. C. Wang, W. Bury, D. A. Gómez-Gualdrón, N. A. Vermeulen, J. E. Mondloch, P. Deria, K. Zhang, P. Z. Moghadam, A. A. Sarjeant, R. Q. Snurr, J. F. Stoddart, J. T. Hupp and O. K. Farha, *J. Am. Chem. Soc.*, 2015, **137**, 3585–3591.
24 X. Sun, J. Gu, Y. Yuan, C. Yu, J. Li, H. Shan, G. Li and Y. Liu, *Inorg. Chem.*, 2019, **58**, 7480–7487.
25 D. Alezi, I. Spanopoulos, C. Tsangarakis, A. Shkurenko, K. Adil, Y. Belmabkhout, M. O'Keeffe, M. Eddaoudi and P. N. Trikalitis, *J. Am. Chem. Soc.*, 2016, **138**, 12767–12770.
26 G. M. Sheldrick, *SHELXTL-NT*, version 5.1, Bruker AXS Inc., Madison, WI, 1997.
27 V. A. Blatov, A. P. Shevchenko and D. M. Proserpio, *Cryst. Growth Des.*, 2014, **14**, 3576–3683.
28 A. K. Rappe, C. J. Casewit, K. S. Colwell, W. A. Goddard and W. M. Skiff, *J. Am. Chem. Soc.*, 1992, **114**, 10024–10035.
29 J. P. Perdew, K. Burke and M. Ernzerhof, *Phys. Rev. Lett.*, 1996, **77**, 3865–3868.
30 H. He, Y. Song, F. Sun, Z. Bian, L. Gao and G. Zhu, *J. Mater. Chem. A*, 2015, **3**, 16598–16603.
31 M. Kandiah, M. H. Nilsen, S. Usseglio, S. Jakobsen, U. Olsbye, M. Tilset, C. Larabi, E. A. Quadrelli, F. Bonino and K. P. Lillerud, *Chem. Mater.*, 2010, **22**, 6632–6640.
32 M. J. Katz, Z. J. Brown, Y. J. Colón, P. W. Siu, K. A. Scheidt, R. Q. Snurr, J. T. Hupp and O. K. Farha, *Chem. Commun.*, 2013, **49**, 9449–9451.
33 G. C. Shearer, S. Chavan, J. Ethiraj, J. G. Vitillo, S. Svelle, U. Olsbye, C. Lamberti, S. Bordiga and K. P. Lillerud, *Chem. Mater.*, 2014, **26**, 4068–4071.
34 M. J. Cliffe, W. Wan, X. Zou, P. A. Chater, A. K. Kleppe, M. G. Tucker, H. Wilhelm, N. P. Funnell, F.-X. Coudert and A. L. Goodwin, *Nat. Commun.*, 2014, **5**, 4176.
35 P. Nugent, Y. Belmabkhout, S. D. Burd, A. J. Cairns, R. Luebke, K. Forrest, T. Pham, S. Ma, B. Space, L. Wojtas, M. Eddaoudi and M. J. Zaworotko, *Nature*, 2013, **495**, 80.
36 D. D. Zhou, C. T. He, P. Q. Liao, W. Xue, W. X. Zhang, H. L. Zhou, J. P. Zhang and X. M. Chen, *Chem. Commun.*, 2013, **49**, 11728–11730.
37 R. Luebke, J. F. Eubank, A. J. Cairns, Y. Belmabkhout, L. Wojtas and M. Eddaoudi, *Chem. Commun.*, 2012, **48**, 1455–1457.

38 B. Wang, X. L. Lv, D. Feng, L. H. Xie, J. Zhang, M. Li, Y. Xie, J. R. Li and H. C. Zhou, *J. Am. Chem. Soc.*, 2016, **138**, 6204–6216.
39 C. S. Liu, Z. H. Zhang, M. Chen, H. Zhao, F. H. Duan, D.-M. Chen, M. H. Wang, S. Zhang and M. Du, *Chem. Commun.*, 2017, **53**, 3941–3944.
40 C. X. Chen, Z. W. Wei, J. J. Jiang, S. P. Zheng, H. P. Wang, Q. F. Qiu, C. C. Cao, D. Fenske and C. Y. Su, *J. Am. Chem. Soc.*, 2017, **139**, 6034–6037.
41 Y. Zhao, S. Qi, Z. Niu, Y. Peng, C. Shan, G. Verma, L. Wojtas, Z. Zhang, B. Zhang, Y. Feng, Y.-S. Chen and S. Ma, *J. Am. Chem. Soc.*, 2019, **141**, 14443–14450.
42 Y.-C. Qiu, S. Yuan, X.-X. Li, D.-Y. Du, C. Wang, J.-S. Qin, H. F. Drake, Y.-Q. Lan, L. Jiang and H.-C. Zhou, *J. Am. Chem. Soc.*, 2019, **141**, 13841–13848.
43 S. Wang, N. Xhaferaj, M. Wahiduzzaman, K. Oyekan, X. Li, K. Wei, B. Zheng, A. Tissot, J. Marrot, W. Shepard, C. Martineau-Corcos, Y. Filinchuk, K. Tan, G. Maurin and C. Serre, *J. Am. Chem. Soc.*, 2019, **141**, 17207–17216.
44 W. Lu, D. Yuan, J. Sculley, D. Zhao, R. Krishna and H. C. Zhou, *J. Am. Chem. Soc.*, 2011, **133**, 18126–18129.
45 S. D. Burd, S. Ma, J. A. Perman, B. J. Sikora, R. Q. Snurr, P. K. Thallapally, J. Tian, L. Wojtas and M. J. Zaworotko, *J. Am. Chem. Soc.*, 2012, **134**, 3663–3666.
46 H. Zhao, Z. Jin, H. Su, J. Zhang, X. Yao, H. Zhao and G. Zhu, *Chem. Commun.*, 2013, **49**, 2780–2782.
47 S. Yao, D. Wang, Y. Cao, G. Li, Q. Huo and Y. Liu, *J. Mater. Chem. A*, 2015, **3**, 16627–16632.
48 Z. Xiang, X. Peng, X. Cheng, X. Li and D. Cao, *J. Phys. Chem. C*, 2011, **115**, 19864–19871.
49 Z. Zhang, S. Xiang, K. Hong, M. C. Das, H. D. Arman, M. Garcia, J. U. Mondal, K. M. Thomas and B. Chen, *Inorg. Chem.*, 2012, **51**, 4947–4953.
50 D. Wang, T. Zhao, Y. Cao, S. Yao, G. Li, Q. Huo and Y. Liu, *Chem. Commun.*, 2014, **50**, 8648–8650.
51 Y. Wang, Z. Hu, T. Kundu, Y. Cheng, J. Dong, Y. Qian, L. Zhai and D. Zhao, *ACS Sustainable Chem. Eng.*, 2018, **6**, 11904–11912.
52 Z. Hu, Y. Wang, S. Farooq and D. Zhao, *AIChE J*, 2017, **63**, 4103–4114.
53 G. E. Cmarik, M. Kim, S. M. Cohen and K. S. Walton, *Langmuir*, 2012, **28**, 15606–15613.
54 Z. Hu, Y. Peng, Z. Kang, Y. Qian and D. Zhao, *Inorg. Chem.*, 2015, **54**, 4862–4868.
55 Z. Li, H. Chen, C. Chen, Q. Guo, X. Li, Y. He, H. Wang, N. Feng, H. Wan and G. Guan, *Chem. Eng. J.*, 2019, **375**, 121962.
56 R. Krishna, *Microporous Mesoporous Mater.*, 2014, **185**, 30–50.
57 R. Krishna, *RSC Adv.*, 2015, **5**, 52269–52295.
58 Z. Hu, B. J. Deibert and J. Li, *Chem. Soc. Rev.*, 2014, **43**, 5815–5840.
59 X. Liu, B. Liu, G. Li and Y. Liu, *J. Mater. Chem. A*, 2018, **6**, 17177–17185.
60 R. Fu, S. Hu and X. Wu, *J. Mater. Chem. A*, 2017, **5**, 1952–1956.
61 A. Gogia and S. K. Mandal, *Dalton Trans.*, 2019, **48**, 2388–2398.
62 P. Das and S. K. Mandal, *J. Mater. Chem. A*, 2018, **6**, 16246–16256.
63 X.-Z. Song, S.-Y. Song, S.-N. Zhao, Z.-M. Hao, M. Zhu, X. Meng, L. L. Wu and H. J. Zhang, *Adv. Funct. Mater.*, 2014, **24**, 4034–4041.

Electronic Supplementary Information

A Multifunctional Double Walled Zirconium Metal-Organic Framework: High Performance of CO_2 Adsorption and Separation, Detecting Explosives in Aqueous Phase

Xiaodong Sun,[a,c] Xu Li,[b] Shuo Yao,[a] Rajamani Krishna,[d] Jiaming Gu,[a] Guanghua Li,[a] Yunling Liu*[a]

[a] *State Key Laboratory of Inorganic Synthesis and Preparative Chemistry, College of Chemistry, Jilin University, Changchun 130012, P. R. China*
[b] *School of Chemical Engineering and Light Industry, Guangdong University of Technology, Guangzhou 510006, Guangdong, P. R. China.*
[c] *Institute of Clean Energy Chemistry, Key Laboratory for Green Synthesis and Preparative Chemistry of Advanved Materials, College of Chemistry, Liaoning University, Shenyang 110036, China*
[d] *Van't Hoff Institute For Molecular Sciences, University of Amsterdam, Science Park 904, 1098 XH Amsterdam, The Netherlands*

Table of contents

1. XRD and TGA characterization of JLU-Liu45

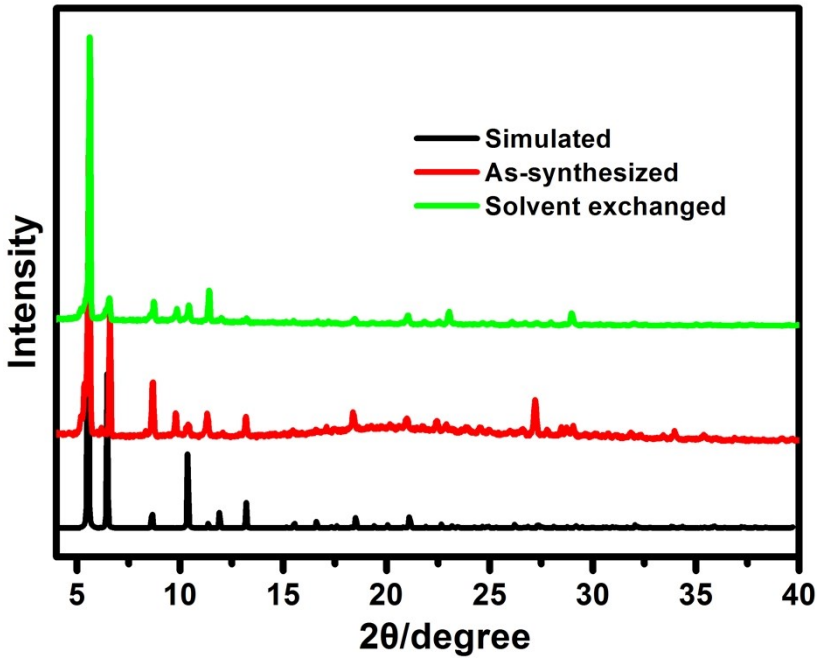

Fig. S1 PXRD patterns of **JLU-Liu45** for simulated, as-synthesized and CH_3CN solvent exchanged sample.

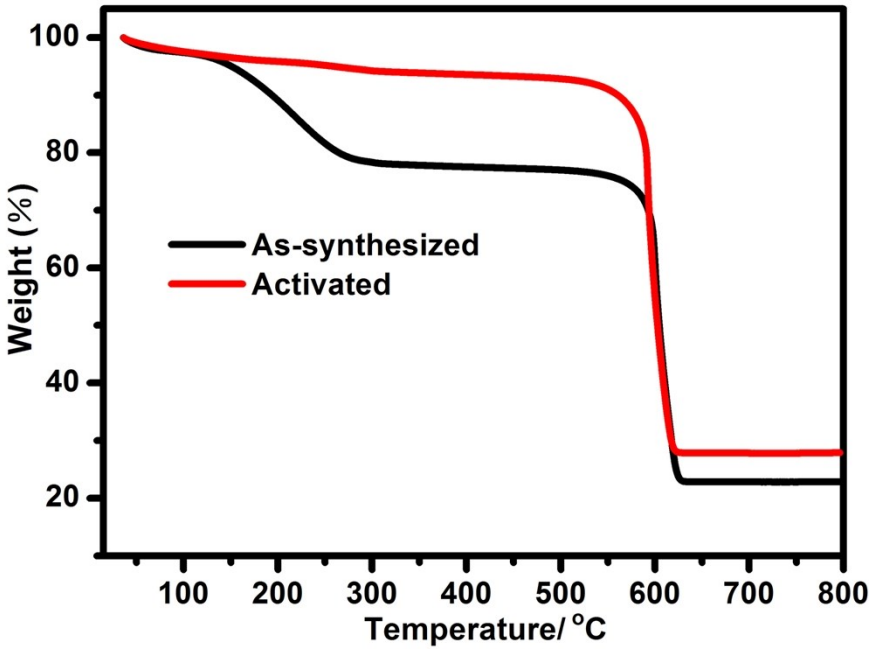

Fig. S2 TGA curves of **JLU-Liu45** for the as-synthesized and activated sample.

2. Structure description of JLU-Liu45

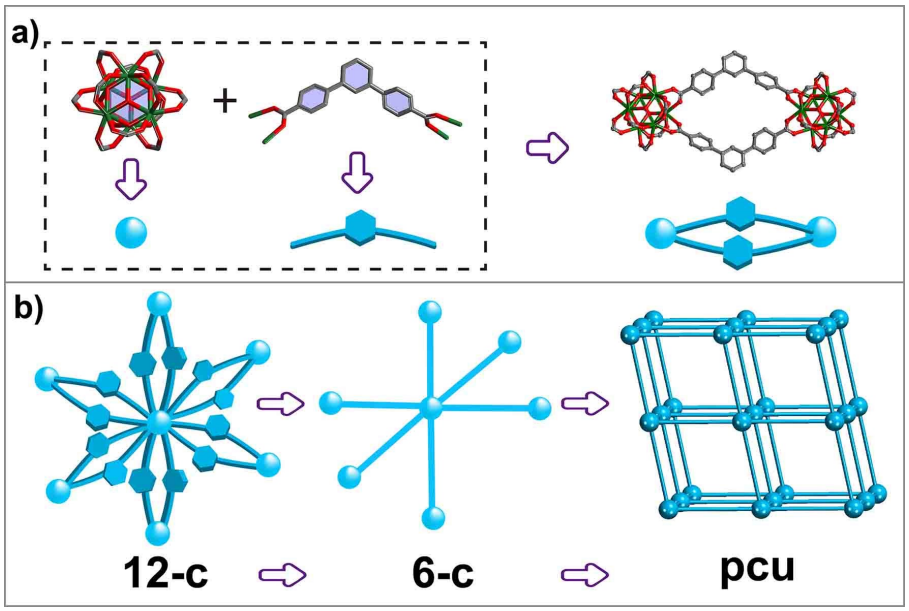

Fig. S3 Double walled building blocks assembled by two $Zr_6O_4(OH)_4(CO_2)_{12}$ SBUs and two C2-symmetric V-shaped H_2DCPB ligands (a); the 12-c building blocks with double wall can be simplified to a 6-c node and form the 6-c network with pcu topology (b). (Color scheme: carbon = grey; oxygen = red; zirconium = dark green).

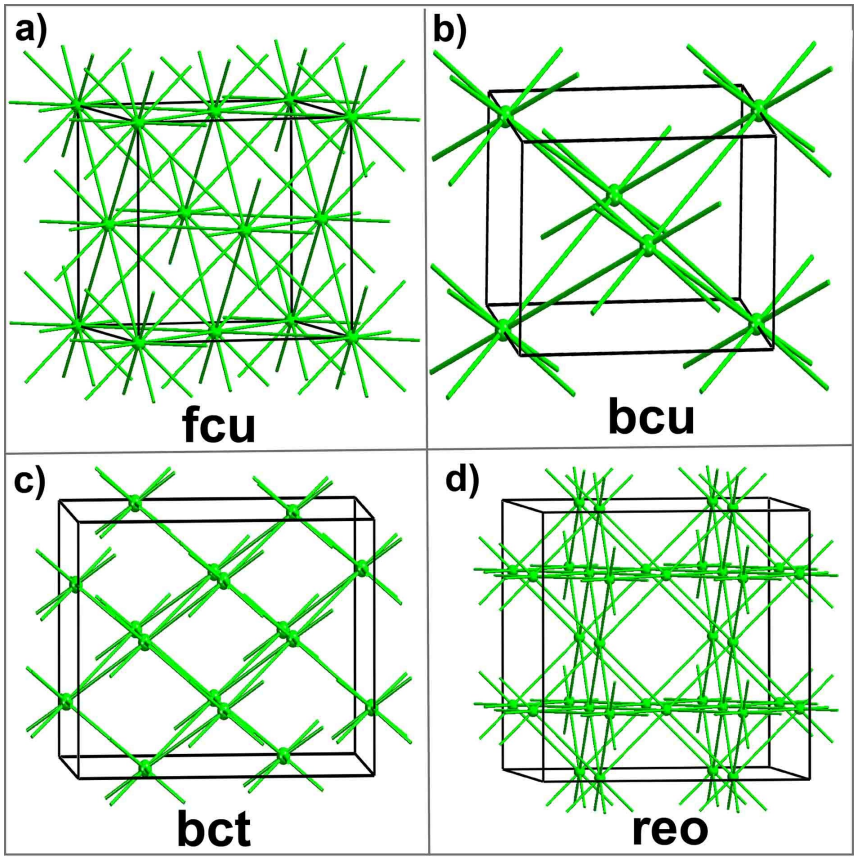

Fig. S4 Representative network topologies in reported Zr-MOFs constructed by dicarboxylate ligands.

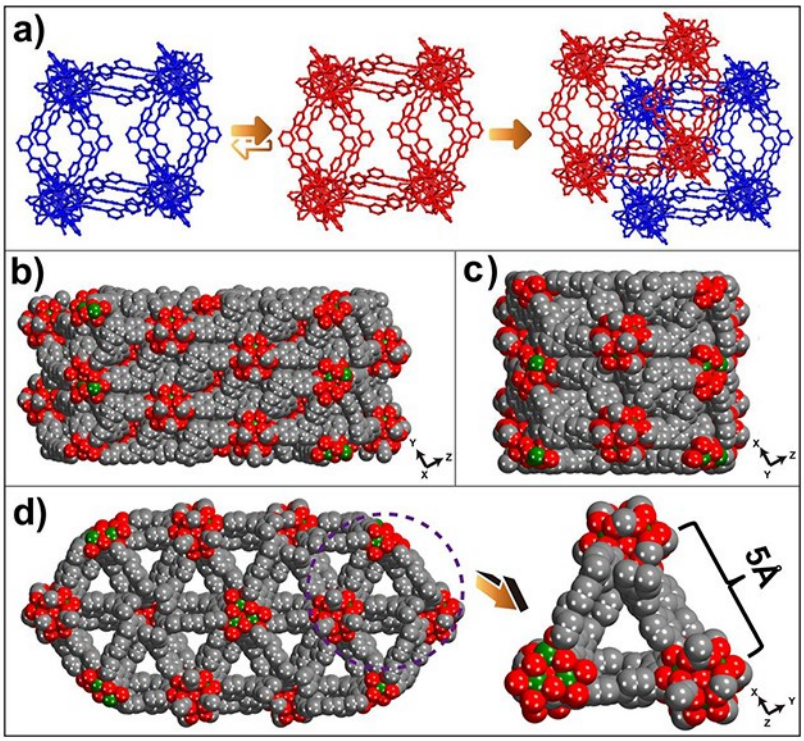

Fig. S5 (a) The formation of 3D interpenetrated framework; (b), (c) and (d) space-filling representations of the structure of **JLU-Liu45** viewed along the [100], [010] and [001] directions, respectively, and the dimension of triangle windows about 5 Å considering the van der Waals radius.

3. Stability test of JLU-Liu45

The thermal and chemical stability of **JLU-Liu45** was examined. The thermal stability was assessed by thermo gravimetric analysis (TGA) under an atmospheric environment. The high decomposition temperature which can reach up to 550 ^{o}C reveals the notable thermal stability of the **JLU-Liu45** material. On the other hand, to estimate the chemical stability of the framework, the as-synthesized **JLU-Liu45** samples were immersed in HCl and NaOH aqueous solutions with a pH range from 0 to 11, and different organic solutions at room temperature for 48 h. The PXRD patterns were completely maintained from the harsh chemical environment. Although slight differences of the peak strength can be observed, the N_2 adsorption measurement of the samples after stability test demonstrated that **JLU-Liu45** exhibited excellent chemical stability. PXRD patterns for **JLU-Liu45** sample before and after measuring the water adsorption isotherm also indicate its water stability. Because of the following reasons, **JLU-Liu45** exhibits commendable stability: (1) Zr^{4+} has high charge density, polarizes the O atoms of the carboxylate groups to form strong Zr-O bonds with significant covalent character. (2) Double walled framework can improve the stability of the material. (3) Interpenetration framework can minimize the empty space and further enhance the stability of the material. In conclusion, **JLU-Liu45** is highly robust and deserves further exploring in practical applications.

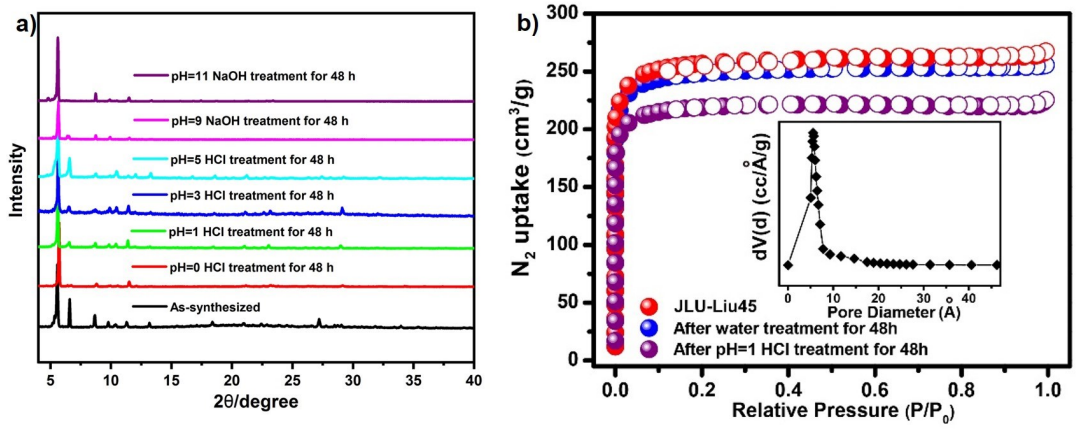

Fig. S6 (a) PXRD patterns and (b) N_2 isotherms of **JLU-Liu45** after immersed in aqueous solutions with different pH values at room temperature for 48 h and the corresponding pore size distribution curve calculated using DFT method (insert).

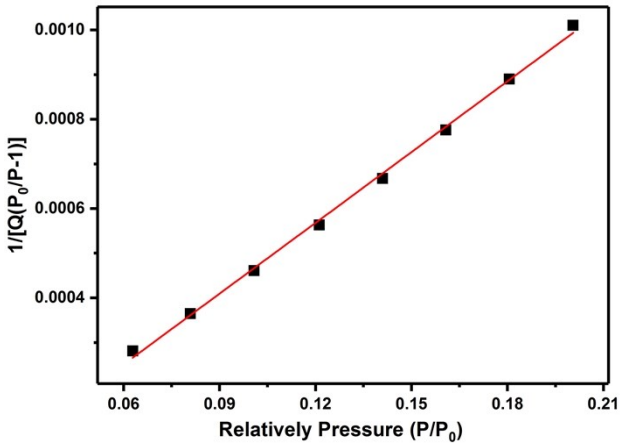

Fig. S7 The linear fitting curve for calculating BET surface areas of **JLU-Liu45**.

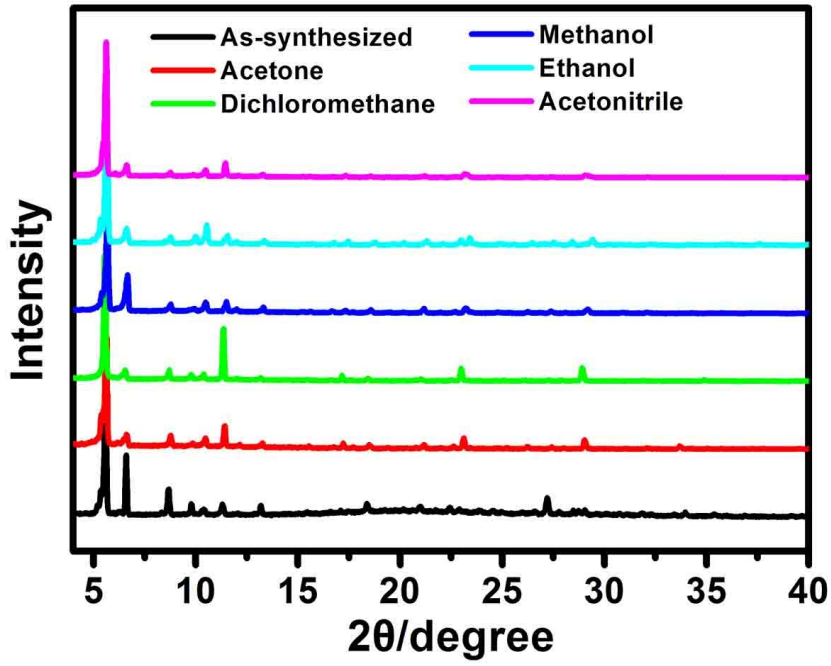

Fig. S8 PXRD patterns of **JLU-Liu45** for as-synthesized and the sample immersed in different organic solutions at room temperature for 48 h.

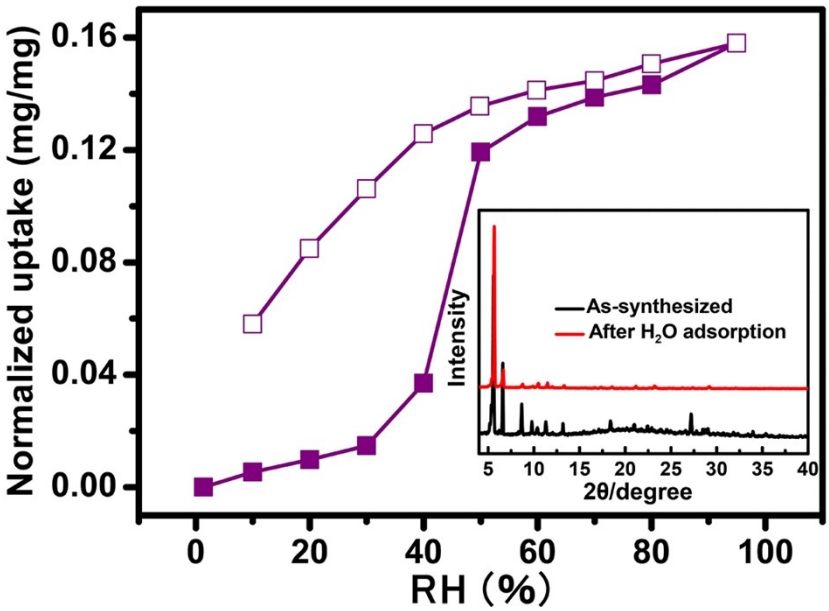

Fig. S9 Water adsorption isotherm of **JLU-Liu45** (experimental condition: T = 298 K, P = 1 bar; N_2 carrier gas). PXRD patterns (insert graph) for **JLU-Liu45** sample before and after measuring the water adsorption isotherm.

4. Gas adsorption and separation studies

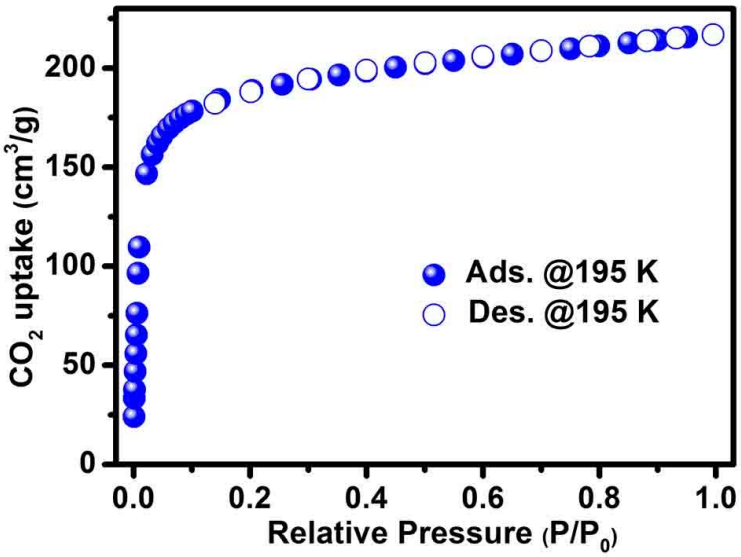

Fig. S10 The CO_2 adsorption isotherm for **JLU-Liu45** at 195 K under 1 bar.

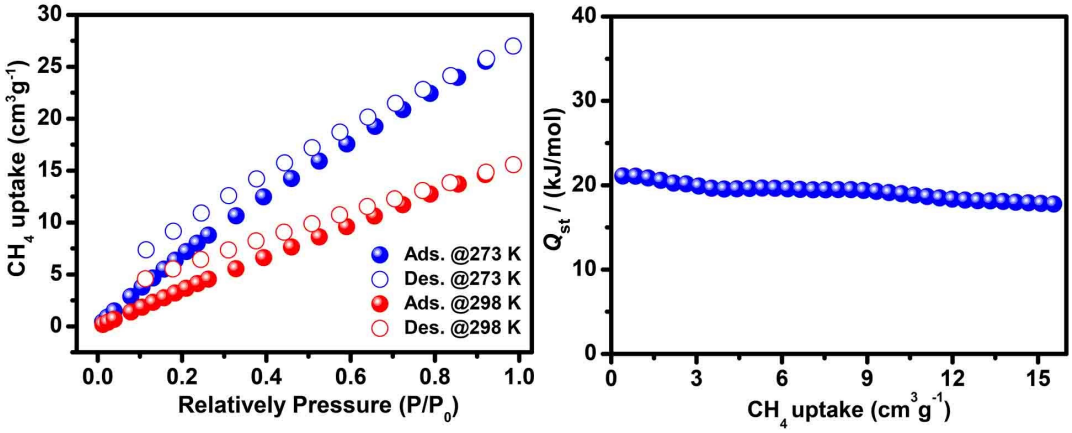

Fig. S11 The CH_4 isotherms for **JLU-Liu45** at 273 and 298 K under 1 bar and Q_{st} of CH_4 for **JLU-Liu45**.

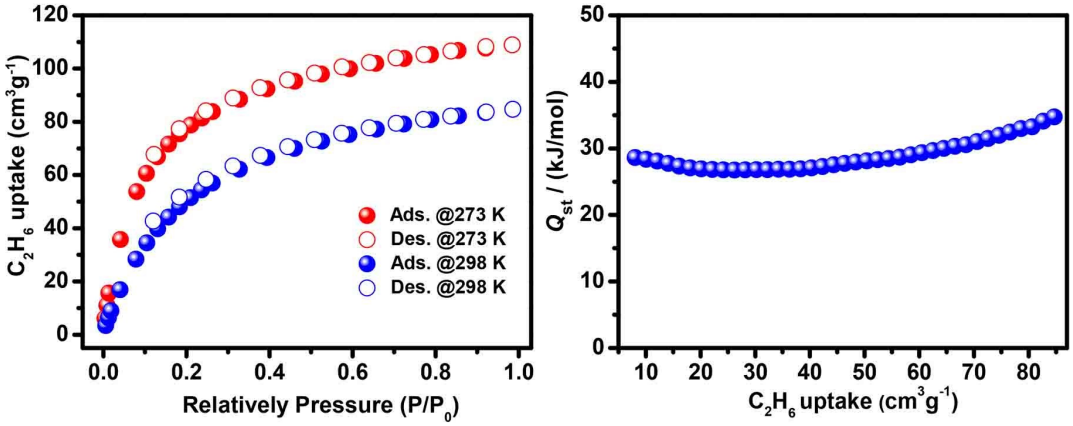

Fig. S12 The C_2H_6 isotherms for **JLU-Liu45** at 273 and 298 K under 1 bar and Q_{st} of C_2H_6 for **JLU-Liu45**.

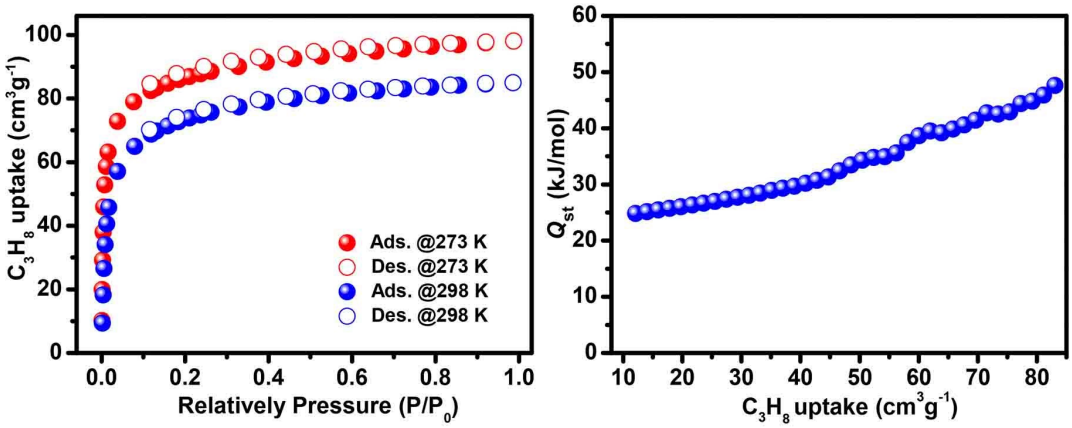

Fig. S13 The C_3H_8 isotherms for **JLU-Liu45** at 273 and 298 K under 1 bar and Q_{st} of C_3H_8 for **JLU-Liu45**.

5. Calculation procedures of selectivity from IAST

The measured experimental data is excess loadings (q^{ex}) of the pure components N_2, CO_2, CH_4, C_2H_6 and C_3H_8 for **JLU-Liu45**, which should be converted to absolute loadings (q) firstly.

$$q = q^{ex} + \frac{pV_{pore}}{ZRT}$$

Here Z is the compressibility factor. The Peng-Robinson equation was used to estimate the value of compressibility factor to obtain the absolute loading, while the measure pore volume 0.38 $cm^3\ g^{-1}$ is also necessary.

The dual-site Langmuir-Freundlich equation is used for fitting the isotherm data at 298 K.

$$q = q_{m_1} \times \frac{b_1 \times p^{1/n_1}}{1 + b_1 \times p^{1/n_1}} + q_{m_2} \times \frac{b_2 \times p^{1/n_2}}{1 + b_2 \times p^{1/n_2}}$$

Here p is the pressure of the bulk gas at equilibrium with the adsorbed phase (kPa), q is the adsorbed amount per mass of adsorbent (mol kg^{-1}), q_{m1} and q_{m2} are the saturation capacities of sites 1 and 2 (mol kg-1), b_1 and b_2 are the affinity coefficients of sites 1 and 2 (1/kPa), n_1 and n_2 are the deviations from an ideal homogeneous surface.

The selectivity of preferential adsorption of component 1 over component 2 in a mixture containing 1 and 2, perhaps in the presence of other components too, can be formally defined as

$$S = \frac{q_1/q_2}{p_1/p_2}$$

q_1 and q_2 are the absolute component loadings of the adsorbed phase in the mixture. These component loadings are also termed the uptake capacities. We calculate the values of q_1 and q_2 using the Ideal Adsorbed Solution Theory (IAST) of Myers and Prausnitz.

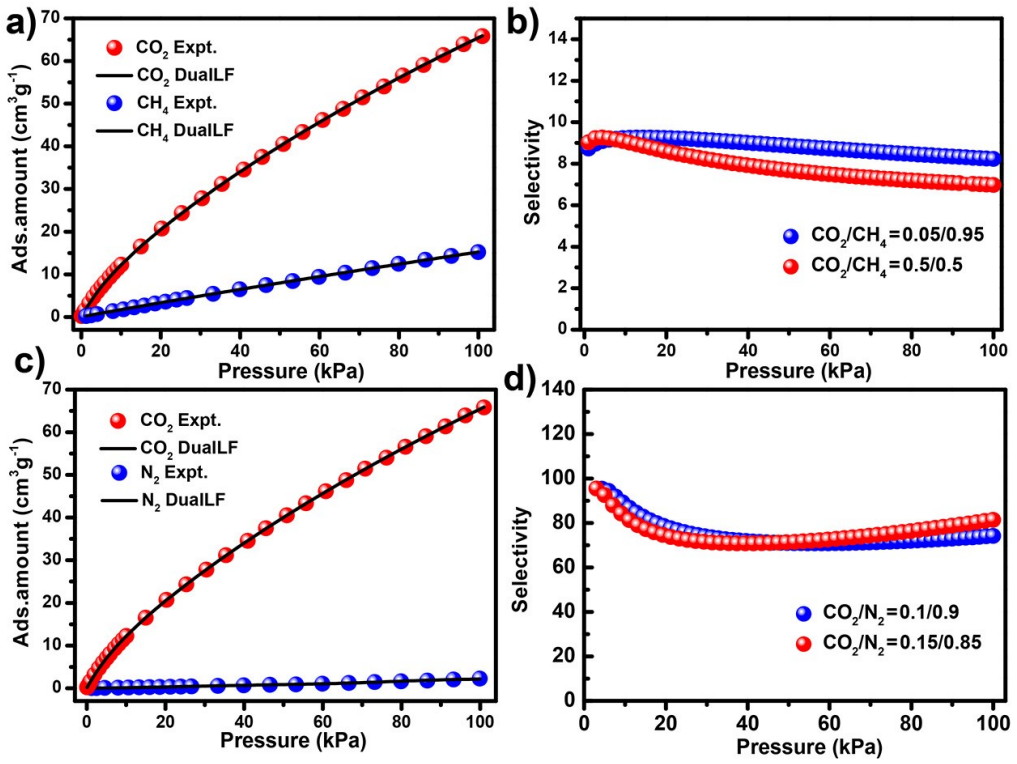

Fig. S14 CO_2, CH_4 and N_2 adsorption isotherms at 298 K along with the dual-site Langmuir Freundlich (DSLF) fits (a and c); gas mixture adsorption selectivity are predicted by IAST at 298 K and 100 kPa for **JLU-Liu45** (b and d).

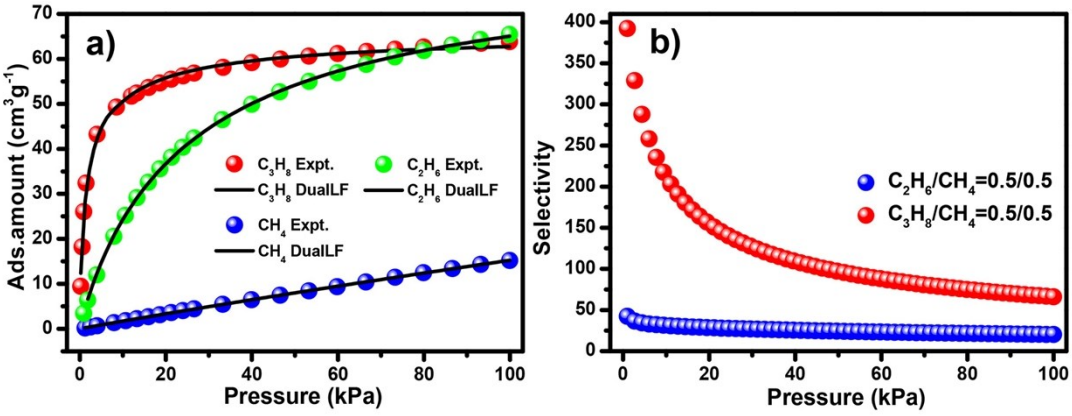

Fig. S15 CH_4, C_2H_6 and C_3H_8 adsorption isotherms at 298 K along with the dual-site Langmuir Freundlich (DSLF) fits (a); gas mixture adsorption selectivity are predicted by IAST at 298 K and 100 kPa for **JLU-Liu45** (b).

6. Transient breakthrough of mixtures in fixed bed adsorbers

The performance of industrial fixed bed adsorbers is dictated by a combination of adsorption selectivity and uptake capacity. For a proper evaluation of the separation performance, we performed transient breakthrough simulations using the simulation methodology described in the literature. For the breakthrough simulations, the following parameter values were used: length of packed bed, L = 0.3 m; voidage of packed bed, ε = 0.4; superficial gas velocity at inlet, u = 0.04 m/s. The transient breakthrough simulation results are presented in terms of a *dimensionless* time, τ, defined by dividing the actual time, t, by the characteristic time, $\frac{L\varepsilon}{u}$.

Notation

c_i	molar concentration of species i in gas mixture at exit of adsorber, mol m^{-3}
c_{i0}	molar concentration of species i in gas mixture at inlet of adsorber, mol m^{-3}
L	length of packed bed adsorber, m
t	time, s
u	superficial gas velocity in packed bed, m s^{-1}

Greek letters

τ	time, dimensionless

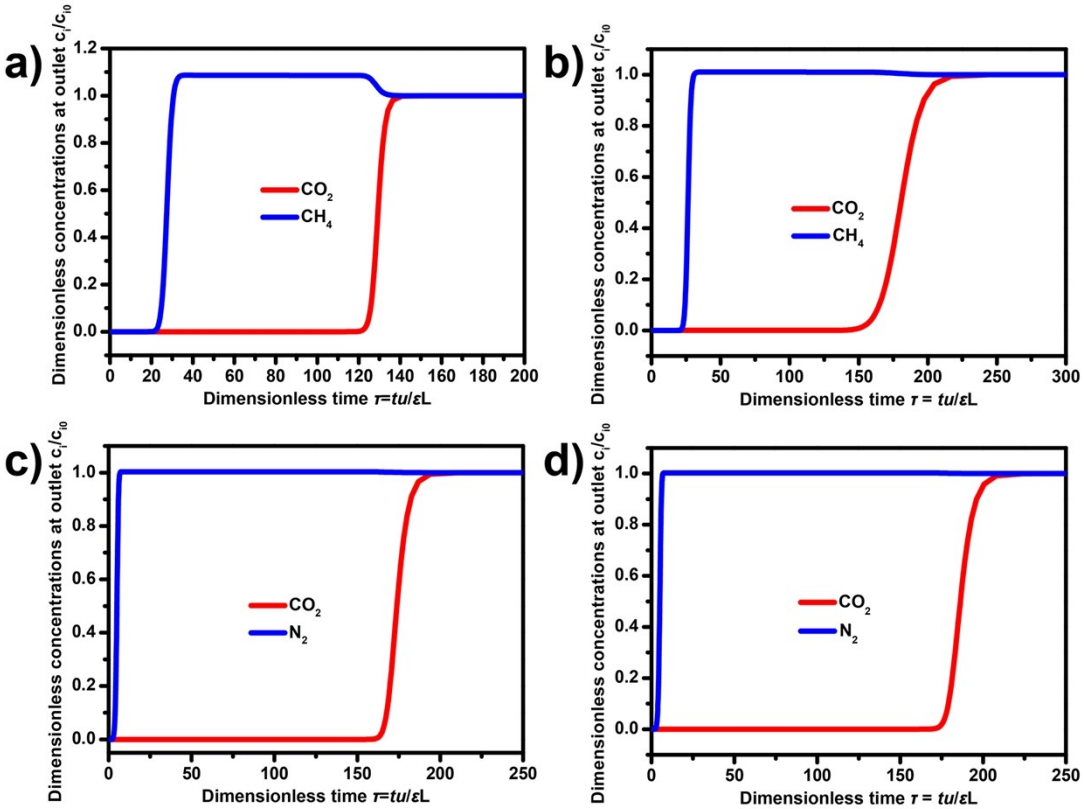

Fig. S16 Transient breakthrough simulations for separation of 50/50 and 5/95 (a and b) CO_2/CH_4, 15/85 and 10/90 (c and d) CO_2/N_2 mixtures containing. The total inlet pressure is 100 kPa. The y-axis is the dimensionless concentrations at the exit, normalized with respect to the inlet concentrations.

7. Computational simulation studies of CO_2 adsorption

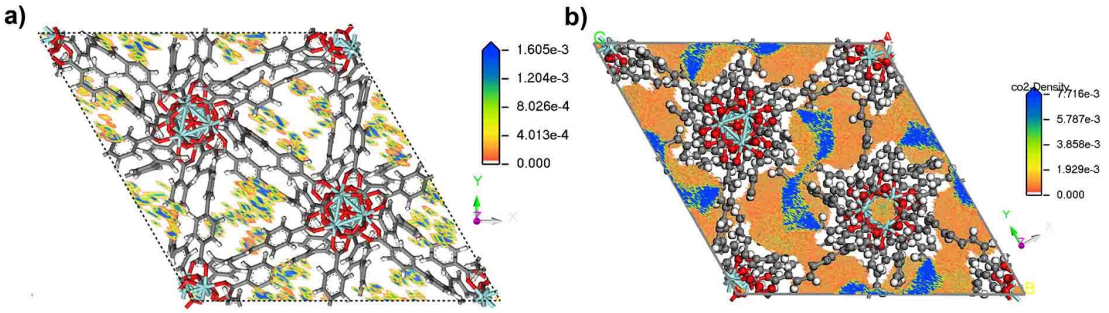

Fig. S17 Density distribution of the center-of-mass of CO_2 molecules in one unit cell of **JLU-Liu45** framework at 298 K and 1 bar simulated by GCMC method (a and b).

8. Detection of selected nitroaromatics

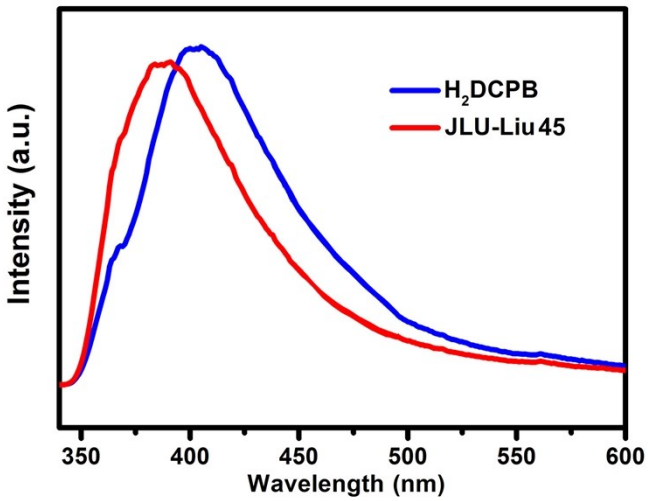

Fig. S18 Solid-state photoluminescent spectra of **JLU-Liu45** and free H_2DCPB ligand excited at 323 nm at room temperature.

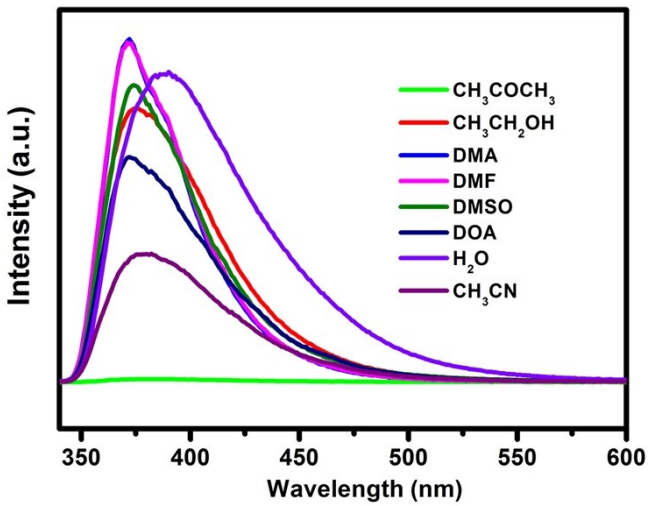

Fig. S19 Photoluminescent spectra of **JLU-Liu45** dispersed in different solvents excited at 323 nm.

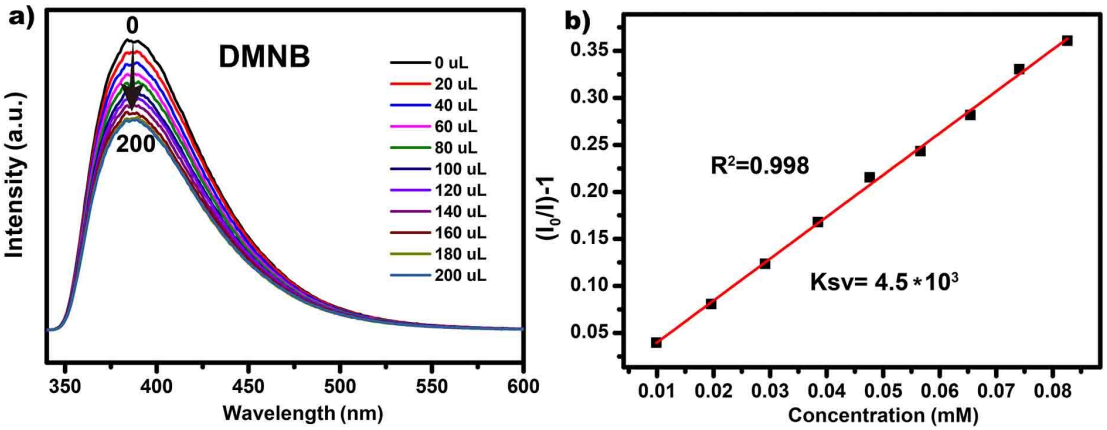

Fig. S20 a) Effect on the emission spectra of **JLU-Liu45** dispersed in water upon the incremental addition of 200 μL (1 mM, 20 μL addition each time) aqueous solution of DMNB. b) SV plot of DMNB.

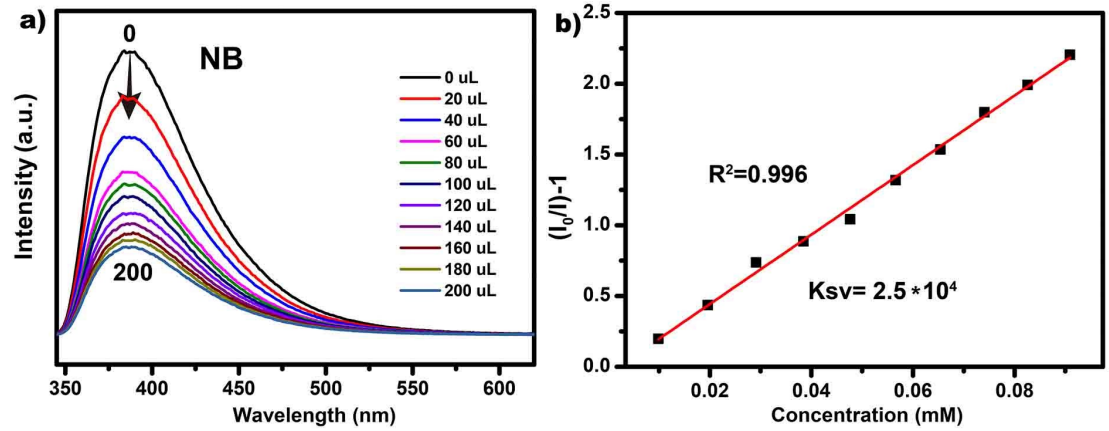

Fig. S21 a) Effect on the emission spectra of **JLU-Liu45** dispersed in water upon the incremental addition of 200 μL (1 mM, 20 μL addition each time) aqueous solution of NB. b) SV plot of NB.

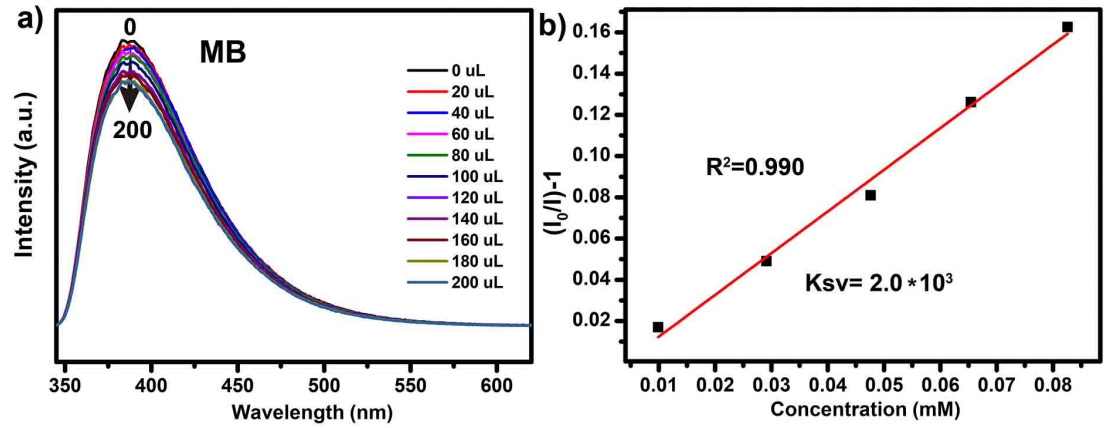

Fig. S22 a) Effect on the emission spectra of **JLU-Liu45** dispersed in water upon the incremental addition of 200 μL (1 mM, 20 μL addition each time) aqueous solution of MB. b) SV plot of MB.

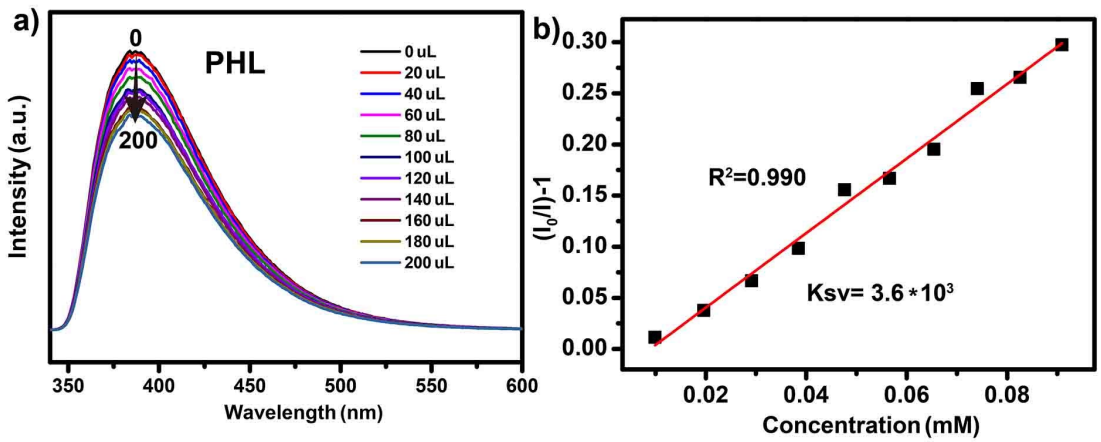

Fig. S23 a) Effect on the emission spectra of **JLU-Liu45** dispersed in water upon the incremental addition of 200 μL (1 mM, 20 μL addition each time) aqueous solution of PHL. b) SV plot of PHL.

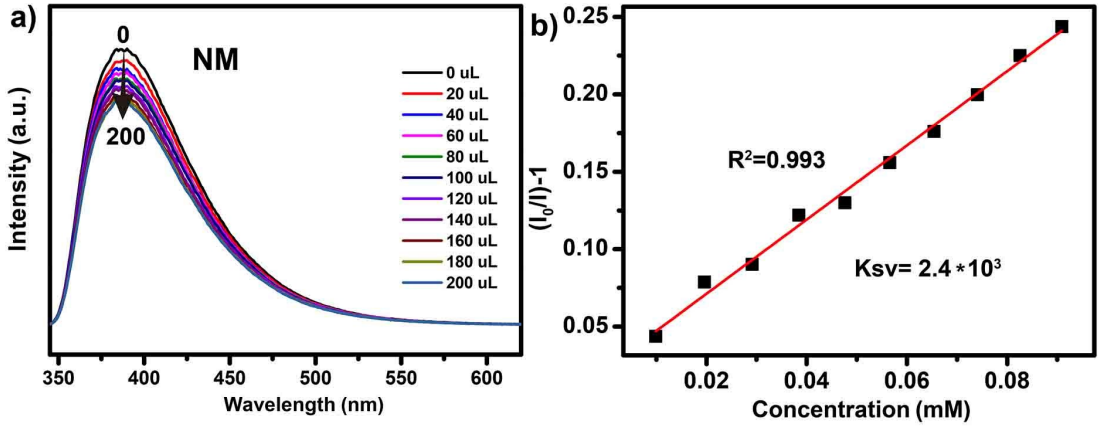

Fig. S24 a) Effect on the emission spectra of **JLU-Liu45** dispersed in water upon the incremental addition of 200 μL (1 mM, 20 μL addition each time) aqueous solution of NM. b) SV plot of NM.

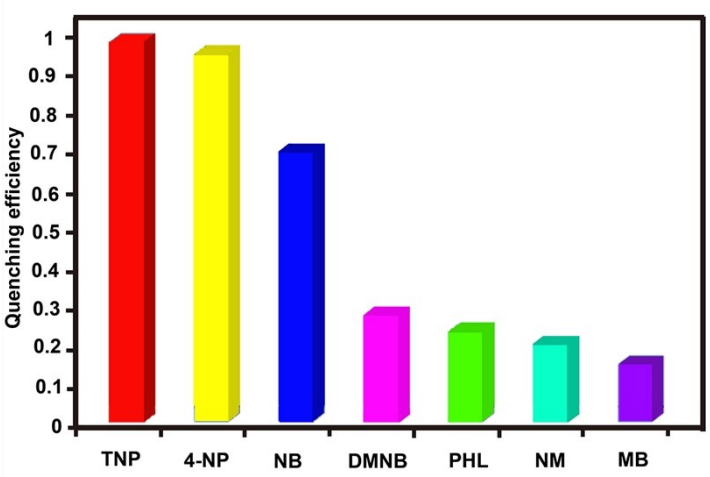

Fig. S25 The fluorescence quenching efficiency for different analytes.

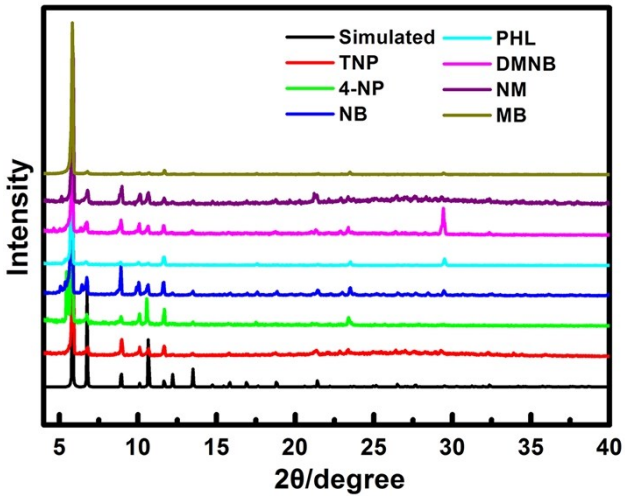

Fig. S26 Powder X-ray diffraction (PXRD) patterns of **JLU-Liu45** after the detection of antibiotics and nitroaromatics.

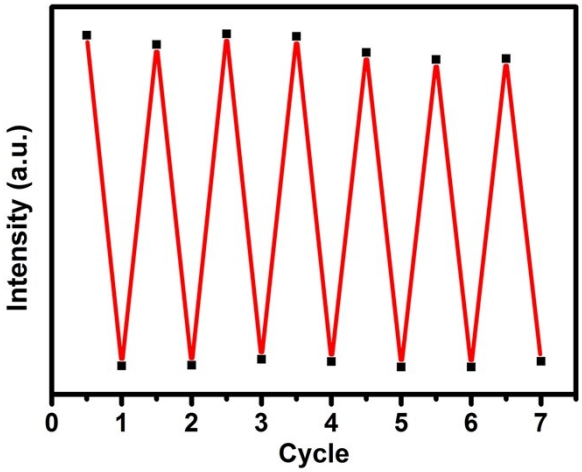

Fig. S27 Reproducibility of the quenching ability of **JLU-Liu45** dispersed in water in the presence of 1 mM aqueous solution of TNP.

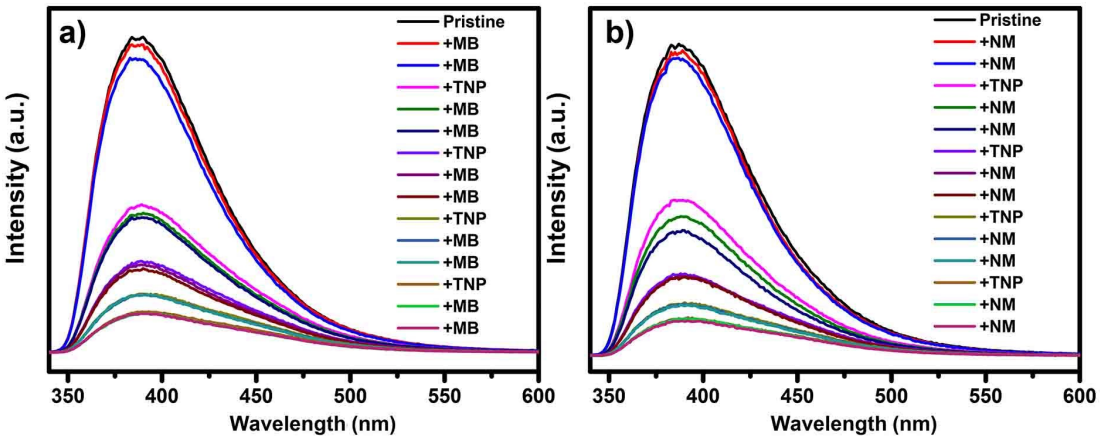

Fig. S28 Tracked emission spectra of **JLU-Liu45** upon the addition of 1 mM aqueous solution of a) MB b) NM followed by 1 mM aqueous solution of TNP, respectively (20 μL addition each time).

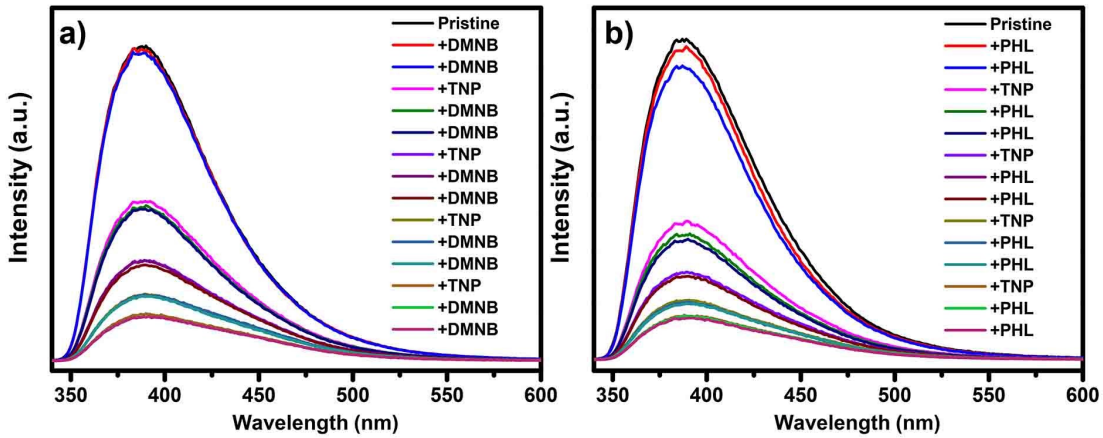

Fig. S29 Tracked emission spectra of **JLU-Liu45** upon the addition of 1 mM aqueous solution of a) DMNB b) PHL followed by 1 mM aqueous solution of TNP, respectively (20 μL addition each time).

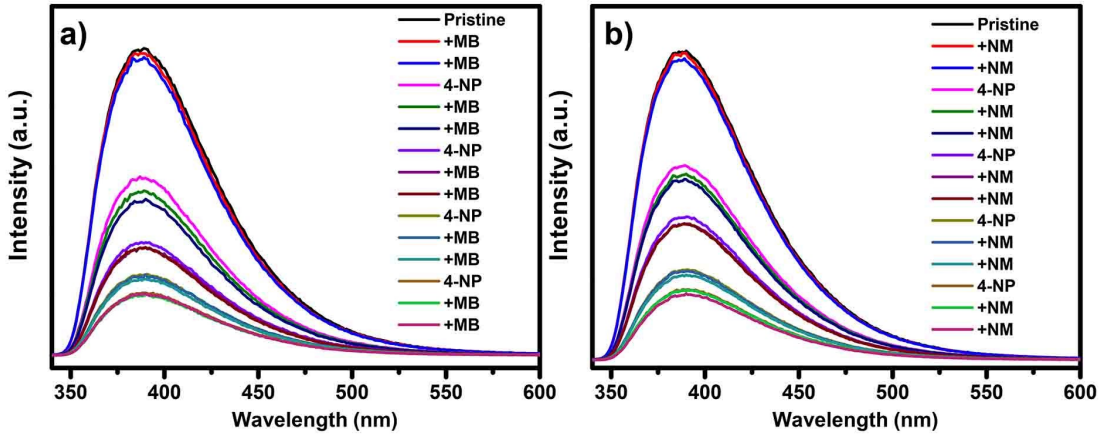

Fig. S30 Tracked emission spectra of **JLU-Liu45** upon the addition of 1 mM aqueous solution of a) MB b) NM followed by 1 mM aqueous solution of 4-NP, respectively (20 μL addition each time).

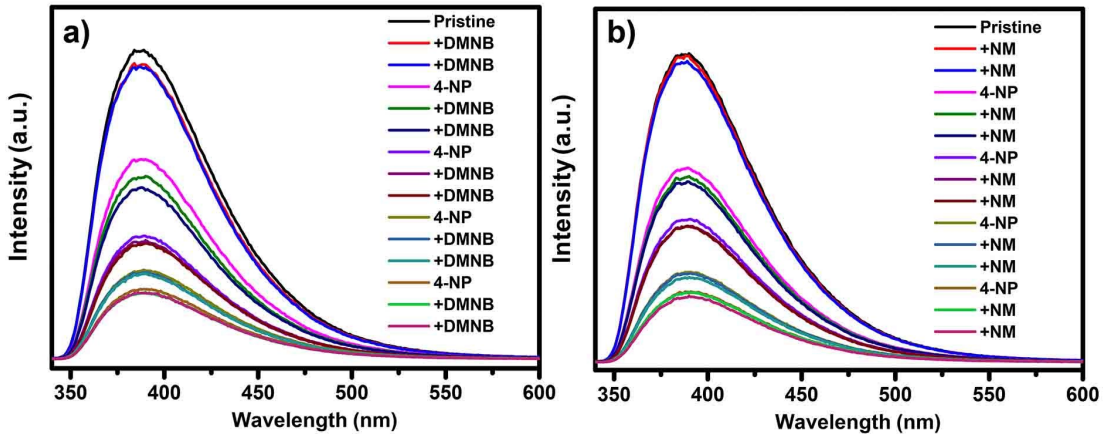

Fig. S31 Tracked emission spectra of **JLU-Liu45** upon the addition of 1 mM aqueous solution of a) DMNB b) PHL followed by 1 mM aqueous solution of 4-NP, respectively (20 μL addition each time).

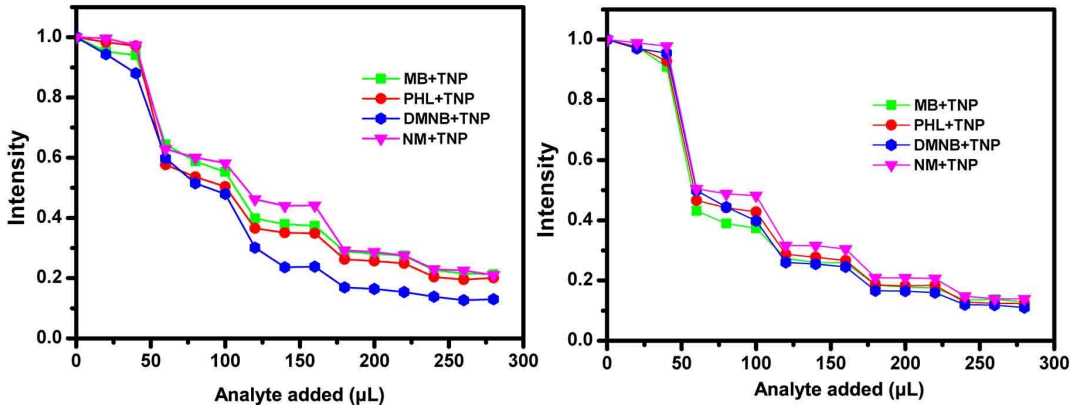

Fig. S32 The selective detection of 4-NP a) and TNP b) on **JLU-Liu45** in the presence of PHL, MB, NM or DMNB in water.

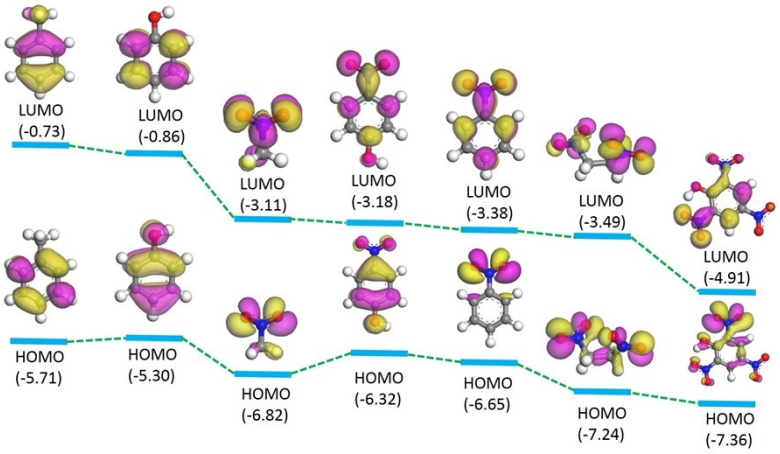

Fig. S33 DFT-calculated HOMO-LUMO energy profiles of MB, PHL, NM, 4-NP, NB, DMNB and TNP (from left to right).

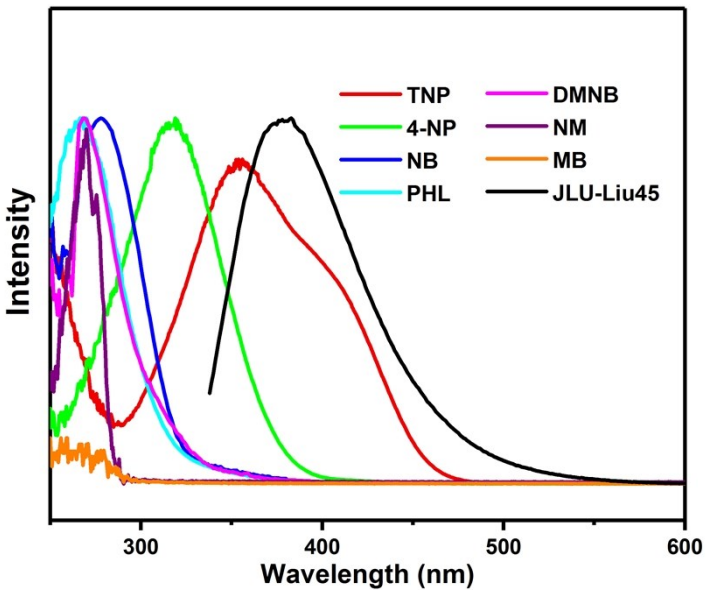

Fig. S34 Spectral overlap between normalized absorption spectra of selected organic explosives and the normalization emission spectrum of **JLU-Liu45**.

9. Tables

Table S1. Crystal data and structure refinement for **JLU-Liu45**

Compound	**JLU-Liu45**
formula	$C_{126}H_{92}N_2O_{35}Zr_6$
formula weight	2741.34
temp (K)	296(2) K
wavelength (Å)	0.71073 Å
crystal system, space group	Trigonal, R-3
a (Å)	30.487(4)
b (Å)	30.487(4)
c (Å)	15.094(3)
V (Å^3)	12150(3)
Z, D_c (Mg/m^3)	6, 1.124
F(000)	4146
θ range (deg)	1.34 to 25.08°
reflns collected/unique	26385/4804
R_{int}	0.0339
data/restraints/params	4804/48/259
GOF on F^2	1.069
R_1, wR_2 (I>2σ(I))	R_1 = 0.0413, wR_2 = 0.1226
R_1, wR_2 (all data)	R_1 = 0.0478, wR_2 = 0.1279

Table S2. Selected bond lengths [Å] and angles [º] for **JLU-Liu45**.

JLU-Liu45			
Zr(1)-O(5')#1	1.959(6)	C(3)-C(4)	1.400(7)
Zr(1)-O(5')	2.097(5)	C(3)-C(14)	1.475(6)
Zr(1)-O(5')#2	2.098(5)	C(5)-C(6)	1.386(6)
Zr(1)-O(6)	2.1341(16)	C(7)-C(12)	1.380(6)
Zr(1)-O(2)#1	2.235(2)	C(17)-C(18)	1.369(5)
Zr(1)-O(5)	2.237(5)	C(17)-C(20)	1.502(5)
C(1)-C(6)	1.381(7)	C(5)-C(4)-C(3)	120.9(4)
C(1)-C(2)	1.389(6)	C(4)-C(3)-C(14)	120.1(4)
O(5')-Zr(1)-O(6)	1.931(4)	C(4)-C(5)-C(6)	120.4(5)
O(5')-Zr(1)#7	2.098(5)	C(12)-C(7)-C(8)	116.9(12)
O(1)-Zr(1)-O(5)#2	142.21(16)	O(4)-C(20)-O(3)	127.3(3)
O(5')#1-Zr(1)-O(3)#3	141.73(16)	O(4)-C(20)-C(17)	116.4(3)
O(5')-Zr(1)-O(3)#3	143.00(17)	O(3)-C(20)-C(17)	116.3(3)
O(5')#2-Zr(1)-O(3)#3	86.01(17)	O(1)-C(13)-O(2)	127.0(3)
O(6)-Zr(1)-O(3)#3	77.22(12)	O(1)-C(13)-C(10)	116.4(3)
O(1)-Zr(1)-O(3)#3	120.78(9)	C(8)-C(7)-C(8')	22.0(14)

Symmetry transformations used to generate equivalent atoms:

#1 y,-x+y,-z #2 -x+y,-x,z #3 x-y+1/3,x-1/3,-z+2/3 #4 -x+1/3,-y+2/3,-z+2/3 #5 x-y,x,-z #6 y+1/3,-x+y+2/3,-z+2/3

Table S3 Force fields parameters of the GCMC simulations.

Atom	σ (Å)	ε/k_B (K)
Zr	2.783	34.691
C	3.473	47.813
O	3.033	48.115
H	2.846	7.642

Table S4 Atomic partial charges of JLU-Liu45 for the GCMC simulations.

JLU-Liu45							
Zr1	0.4989	C61	-0.0518	C121	-0.0169	C181	-0.0596
O2	-0.1974	H62	0.04	C122	-0.0626	H182	0.0325
O3	-0.1984	C63	-0.0672	H123	0.0373	C183	-0.0457
O4	-0.1995	H64	0.0372	C124	-0.0121	H184	0.0394
O5	-0.198	C65	0.1801	C125	-0.0504	C185	-0.0183
O6	-0.3316	C66	-0.0168	H126	0.0459	C186	-0.0487
C7	-0.0169	C67	-0.0596	C127	-0.0484	H187	0.0432
C8	-0.0626	H68	0.0325	H128	0.0551	C188	-0.0618
H9	0.0373	C69	-0.0457	C129	-0.0631	H189	0.0385
C10	-0.0121	H70	0.0394	H130	0.0406	C190	0.1837
C11	-0.0504	C71	-0.0183	C131	-0.0201	Z191	0.4989
H12	0.0459	C72	-0.0487	C132	-0.0658	O192	-0.1973
C13	-0.0484	H73	0.0432	H133	0.036	O193	-0.1985
H14	0.0551	C74	-0.0618	C134	-0.0502	O194	-0.1995
C15	-0.0631	H75	0.0385	H135	0.0417	O195	-0.198
H16	0.0406	C76	0.1837	C136	-0.0215	O196	-0.3317
C17	-0.0201	Z77	0.4989	C137	-0.0517	C197	-0.0169
C18	-0.0658	O78	-0.1973	H138	0.0401	C198	-0.0625
H19	0.036	O79	-0.1985	C139	-0.0672	H199	0.0373
C20	-0.0502	O80	-0.1995	H140	0.0372	C200	-0.012
H21	0.0417	O81	-0.198	C141	0.1801	C201	-0.0504
C22	-0.0215	O82	-0.3317	C142	-0.0167	H202	0.0459
C23	-0.0517	C83	-0.0169	C143	-0.0595	C203	-0.0483
H24	0.0401	C84	-0.0625	H144	0.0325	H204	0.0552
C25	-0.0672	H85	0.0373	C145	-0.0455	C205	-0.0631
H26	0.0372	C86	-0.012	H146	0.0393	H206	0.0406
C27	0.1801	C87	-0.0504	C147	-0.0182	C207	-0.02
C28	-0.0167	H88	0.0459	C148	-0.0486	C208	-0.0657
C29	-0.0595	C89	-0.0483	H149	0.0432	H209	0.0361
H30	0.0325	H90	0.0552	C150	-0.0617	C210	-0.0501
C31	-0.0455	C91	-0.0631	H151	0.0385	H211	0.0418
H32	0.0393	H92	0.0406	C152	0.1838	C212	-0.0214
C33	-0.0182	C93	-0.02	Z153	0.4991	C213	-0.0517
C34	-0.0486	C94	-0.0657	O154	-0.1973	H214	0.0401
H35	0.0432	H95	0.0361	O155	-0.1984	C215	-0.0671

C36	-0.0617	C96	-0.0501	O156	-0.1994	H216	0.0372
H37	0.0385	H97	0.0418	O157	-0.1981	C217	0.1801
C38	0.1838	C98	-0.0214	O158	-0.3317	C218	-0.0167
Z39	0.4991	C99	-0.0517	C159	-0.0169	C219	-0.0594
O40	-0.1973	H100	0.0401	C160	-0.0626	H220	0.0324
O41	-0.1984	C101	-0.0671	H161	0.0373	C221	-0.0456
O42	-0.1994	H102	0.0372	C162	-0.0121	H222	0.0393
O43	-0.1981	C103	0.1801	C163	-0.0504	C223	-0.0182
O44	-0.3317	C104	-0.0167	H164	0.0459	C224	-0.0485
C45	-0.0169	C105	-0.0594	C165	-0.0484	H225	0.0431
C46	-0.0626	H106	0.0324	H166	0.0551	C226	-0.0617
H47	0.0373	C107	-0.0456	C167	-0.0632	H227	0.0385
C48	-0.0121	H108	0.0393	H168	0.0406	C228	0.1837
C49	-0.0504	C109	-0.0182	C169	-0.0201	O229	-0.3337
H50	0.0459	C110	-0.0485	C170	-0.0659	O230	-0.3337
C51	-0.0484	H111	0.0431	H171	0.036		
H52	0.0551	C112	-0.0617	C172	-0.0502		
C53	-0.0632	H113	0.0385	H173	0.0417		
H54	0.0406	C114	0.1837	C174	-0.0215		
C55	-0.0201	Z115	0.4989	C175	-0.0518		
C56	-0.0659	O116	-0.1974	H176	0.04		
H57	0.036	O117	-0.1984	C177	-0.0672		
C58	-0.0502	O118	-0.1995	H178	0.0372		
H59	0.0417	O119	-0.198	C179	0.1801		
C60	-0.0215	O120	-0.3316	C180	-0.0168		

Table S5 A comparison of chemical stability of JLU-Liu45 with other stable Zr-MOFs materials.

Compound	pH values	Reference
JLU-Liu45	0-11	This work
PCN-223	0-10	1
PCN-777	3-11	2
PCN-56	2-11	3
PCN-59	2-11	3
PCN-225	0-12	4
BUT-12	0-10	5
BUT-13	0-10	5
BUT-14	0-10	6
BUT-15	0-10	6
NPF-200	1-12	7
PCN-134	0-13	8

Table S6. CO_2 adsorption capacities and Q_{st} values in reported Zr-MOFs at 273 K and 1 bar.

Zr-MOFs	BET surface area ($m^2\ g^{-1}$)	CO_2 uptake (273 K, $cm^3\ g^{-1}$)	CO_2 uptake (298 K)	Q_{st} values ($kJ\ mol^{-1}$)	Ref.
JLU-Liu45	**971**	**116**	**66**	**34**	**This work**
BUT-10	1310	92	53.5	22	9
BUT-11	1848	89	50.6	26	9
UiO-67	2505	N.A.	22.9	16	9
493-MOF-TATB	820	97	60	25	10
493-MOF-BA	1265	78	50	23	10
493-MOF-NA	1199	85	56	20	10
LIFM-28np	940	29.0	N.A.	22	11
LIFM-79	1689	76.3	~42	32	11
LIFM-77	1619	81.0	~44	34	11
PCN-56	3741	~58	~37[a]	20	3
PCN-57	2572	~50	~33[a]	22	3
PCN-58	2185	~63	~40[a]	24	3
PCN-59	1279	~71	~42[a]	32	3
NU-1000	2320	N.A.	~40[b]	17	12
SALI-9	870	N.A.	~18[b]	34	12
SALI-1’	1600	N.A.	~34[b]	21	12
CPM-99(H_2)	N.A.	73	~50	N.A.	13
CPM-99(Zn)	N.A.	60	~35	N.A.	13
CPM-99(Co)	N.A.	61	~42	N.A.	13
CPM-99(Fe)	1030	76	~45	N.A.	13
MOF-892	1431	~41	~22	24	14
MOF-893	558	~40	~21	31	14
JLU-MOF50	1101	69	35	25	15
JLU-MOF58	3663	49	28	19	16
Corrole-MOF-1	2545	76	46	N.A.	17
PCN-138	1261	63	41	N.A.	18
MIP-203-F	430	61	46	32	19
MIP-203-S	no	36	15	34	19
MIP-203-M	380	48	36	33	19

[a]at 296 K, [b]at 293 K.

Table S7. Gas adsorption data for **JLU-Liu45**.

Compound	N_2[a]		CO_2[a]			CH_4[a]	
	77 K	298 K	195 K	273 K	298 K	273 K	298 K
JLU-Liu45	256	3	216	116	66	27	16
Compound	C_2H_6[a]		C_3H_8[a]			H_2O	
	273 K	298 K	273 K	298 K		298 K	
JLU-Liu45	85	65	74	63		0.16 mg/mg	

[a] Gas uptake in $cm^3\ g^{-1}$.

Table S8. Comparison of CO_2/N_2 (0.15/0.85) selectivity of **JLU-Liu45** with other stable MOFs.

Zr-MOFs	CO_2/N_2 selectivity	Ref.
JLU-Liu45	**81.4**	**This work**
MIL-101	12.6	20
MIL-125-NH_2	27.0	21
MIL-68-Al	37.0	22
ZIF-68	18.0	23
ZIF-69	20.0	23
ZIF-70	17.0	23
ZIF-79	23.0	23
ZIF-81	24.0	23
ZIF-95	18.0	24
UiO-66(Br)	25.1	25
UiO-66(NO_2)	26.4	25
UiO-66	13.4	25
UiO-67	9.4	9
BUT-10	18.6	9
BUT-11	31.5	9
BUT-11(AcOH)	24.1	26
LIFM-77	34.7	11
LIFM-79	25.2	11
LIFM-28np	5.5	11
MIP-203-F	15	19
MIP-203-S	34	19
MIP-203-M	51	19
UiO-66(Zr)-$(OH)_2$	66	27
UiO-66(Zr)-$(OAc)_2$	42.5	27
UiO-66(Zr)-(OPr)2	39.1	27
Opt-UiO-66(Zr)-$(OH)_2$	44.5	28
UiO-66-NH_2	32.3	29
UiO-66(Zr)-$(COOH)_2$	35.4	30
75PEI@meso-UiO-66-0.2Cu	59.4	31
UiO-66(Zr)-$(COOK)_2$	69.3	32
UiO-66(Zr)-$(COONa)_2$	58.0	32

Table S9. Comparison of CO_2/CH_4 (0.5/0.5) selectivity of **JLU-Liu45** with other MOFs materials.

MOFs material	CO_2/CH_4 selectivity	Ref.
JLU-Liu45	7.0	This work
MOF-177	0.9	33
ZIF-8	1.4	33
$Cu_3(BTC)_2$	2.3	33
NOTT-125	4.8	34
FJI-C1	5.9	35
ZJNU-59	6.0	36
NOTT-122	6.4	37
ZJNU-40	6.6	38
ZJNU-69	7.1	39
BSF-1	7.5	40
MFM-126	11.7	41
SNIFSIX-1-Cu	12.1	42

Table S10. Comparison of detection ability of **JLU-Liu45** towards TNP in the water with other materials.

Material	Quenching constant (K_{SV}) for TNP	Ref.
JLU-Liu45	**2.3×10^5 M^{-1}**	**This work**
UiO-67@N	2.9×10^4 M^{-1}	43
$[Eu_3(L)_3(HCOO)(\mu_3\text{-}OH)_2(H_2O)]\cdot x(solv)$	2.1×10^4 M^{-1}	44
UiO-68@NH_2	5.8×10^4 M^{-1}	45
BUT-12	3.1×10^5 M^{-1}	5
BUT-13	5.1×10^5 M^{-1}	5
$[Cd(NDC)L]_2\cdot H_2O$	3.7×10^4 M^{-1}	46
$[Zn_4(DMF)(Ur)_2(NDC)_4]$	10.8×10^4 M^{-1}	47
$[Zn_8(ad)_4(BPDC)_6O\cdot2Me_2NH_2]\cdot G$	4.6×10^4 M^{-1}	48
$[Zn(NDC)(H_2O)]n$	6×10^4 M^{-1}	49
$[Cd(NDC)_{0.5}(PCA)]\cdot xG$	3.5×10^4 M^{-1}	50
In-ADBA	1.3×10^5 M^{-1}	51
$[Tb_2(H_2L)_3(H_2O)_2]\cdot21H_2O$	1.5×10^4 M^{-1}	52
$[Cd_2(tdz)_2(4,4'\text{-}bpy)_2]\cdot6.5H_2O$	4.9×10^4 M^{-1}	53
TFPC-NDA-COF	2.5×10^5 M^{-1}	54

10. REFERENCES

1. D. Feng, Z. Y. Gu, Y. P. Chen, J. Park, Z. Wei, Y. Sun, M. Bosch, S. Yuan and H. C. Zhou, *J. Am. Chem. Soc.*, 2014, **136**, 17714-17717.
2. D. Feng, K. Wang, J. Su, T. F. Liu, J. Park, Z. Wei, M. Bosch, A. Yakovenko, X. Zou and H. C. Zhou, *Angew. Chem. Int. Ed.*, 2015, **54**, 149-154.
3. H. L. Jiang, D. Feng, T. F. Liu, J. R. Li and H. C. Zhou, *J. Am. Chem. Soc.*, 2012, **134**, 14690-14693.
4. H. L. Jiang, D. Feng, K. Wang, Z. Y. Gu, Z. Wei, Y. P. Chen and H. C. Zhou, *J. Am. Chem. Soc.*, 2013, **135**, 13934-13938.
5. B. Wang, X. L. Lv, D. Feng, L. H. Xie, J. Zhang, M. Li, Y. Xie, J. R. Li and H. C. Zhou, *J. Am.*

Chem. Soc., 2016, **138**, 6204-6216.

6. B. Wang, Q. Yang, C. Guo, Y. Sun, L. H. Xie and J. R. Li, *ACS Appl. Mater. Interfaces*, 2017, **9**, 10286-10295.

7. X. Zhang, X. Zhang, J. A. Johnson, Y. S. Chen and J. Zhang, *J. Am. Chem. Soc.*, 2016, **138**, 8380-8383.

8. S. Yuan, J. S. Qin, L. Zou, Y. P. Chen, X. Wang, Q. Zhang and H. C. Zhou, *J. Am. Chem. Soc.*, 2016, **138**, 6636-6642.

9. B. Wang, H. Huang, X. L. Lv, Y. Xie, M. Li and J. R. Li, *Inorg. Chem.*, 2014, **53**, 9254-9259.

10. C. S. Liu, Z. H. Zhang, M. Chen, H. Zhao, F. H. Duan, D.-M. Chen, M. H. Wang, S. Zhang and M. Du, *Chem. Commun.*, 2017, **53**, 3941-3944.

11. C. X. Chen, Z. W. Wei, J. J. Jiang, S. P. Zheng, H. P. Wang, Q. F. Qiu, C. C. Cao, D. Fenske and C. Y. Su, *J. Am. Chem. Soc.*, 2017, **139**, 6034-6037.

12. P. Deria, J. E. Mondloch, E. Tylianakis, P. Ghosh, W. Bury, R. Q. Snurr, J. T. Hupp and O. K. Farha, *J. Am. Chem. Soc.*, 2013, **135**, 16801-16804.

13. Q. Lin, X. Bu, A. Kong, C. Mao, X. Zhao, F. Bu and P. Feng, *J. Am. Chem. Soc.*, 2015, **137**, 2235-2238.

14. P. T. K. Nguyen, H. T. D. Nguyen, H. N. Nguyen, C. A. Trickett, Q. T. Ton, E. Gutiérrez-Puebla, M. A. Monge, K. E. Cordova and F. Gándara, *ACS Appl. Mater. Interfaces*, 2018, **10**, 733-744.

15. X. Sun, S. Yao, C. Yu, G. Li, C. Liu, Q. Huo and Y. Liu, *J. Mater. Chem.A*, 2018, **6**, 6363-6369.

16. X. Sun, J. Gu, Y. Yuan, C. Yu, J. Li, H. Shan, G. Li and Y. Liu, *Inorg. Chem.*, 2019, **58**, 7480-7487.

17. Y. Zhao, S. Qi, Z. Niu, Y. Peng, C. Shan, G. Verma, L. Wojtas, Z. Zhang, B. Zhang, Y. Feng, Y.-S. Chen and S. Ma, *J. Am. Chem. Soc.*, 2019, **141**, 14443-14450.

18. Y.-C. Qiu, S. Yuan, X.-X. Li, D.-Y. Du, C. Wang, J.-S. Qin, H. F. Drake, Y.-Q. Lan, L. Jiang and H.-C. Zhou, *J. Am. Chem. Soc.*, 2019, **141**, 13841-13848.

19. S. Wang, N. Xhaferaj, M. Wahiduzzaman, K. Oyekan, X. Li, K. Wei, B. Zheng, A. Tissot, J. Marrot, W. Shepard, C. Martineau-Corcos, Y. Filinchuk, K. Tan, G. Maurin and C. Serre, *J. Am. Chem. Soc.*, 2019, **141**, 17207-17216.

20. K. Munusamy, G. Sethia, D. V. Patil, P. B. Somayajulu Rallapalli, R. S. Somani and H. C. Bajaj, *Chem. Eng. J.*, 2012, **195-196**, 359-368.

21. S. N. Kim, J. Kim, H. Y. Kim, H. Y. Cho and W. S. Ahn, *Catal. Today*, 2013, **204**, 85-93.

22. Q. Yang, S. Vaesen, M. Vishnuvarthan, F. Ragon, C. Serre, A. Vimont, M. Daturi, G. De Weireld and G. Maurin, *J. Mater. Chem.*, 2012, **22**, 10210-10220.

23. R. Banerjee, H. Furukawa, D. Britt, C. Knobler, M. O'Keeffe and O. M. Yaghi, *J. Am. Chem. Soc.*, 2009, **131**, 3875-3877.

24. B. Wang, A. P. Côté, H. Furukawa, M. O'Keeffe and O. M. Yaghi, *Nature*, 2008, **453**, 207.

25. W. Zhang, H. Huang, C. Zhong and D. Liu, *PCCP*, 2012, **14**, 2317-2325.

26. P. Xydias, I. Spanopoulos, E. Klontzas, G. E. Froudakis and P. N. Trikalitis, *Inorg. Chem.*, 2014, **53**, 679-681.

27. Y. Wang, Z. Hu, T. Kundu, Y. Cheng, J. Dong, Y. Qian, L. Zhai and D. Zhao, *ACS Sustainable Chem. Eng.*, 2018, 6, 11904-11912.

28. Z. Hu, Y. Wang, S. Farooq and D. Zhao, *AlChE J.*, 2017, 63, 4103-4114.

29. G. E. Cmarik, M. Kim, S. M. Cohen and K. S. Walton, *Langmuir*, 2012, 28, 15606-15613.

30. Z. Hu, Y. Peng, Z. Kang, Y. Qian and D. Zhao, *Inorg. Chem.*, 2015, 54, 4862-4868.

31. Z. Li, H. Chen, C. Chen, Q. Guo, X. Li, Y. He, H. Wang, N. Feng, H. Wan and G. Guan, *Chem. Eng. J.*, 2019, 375, 121962.
32. Z. Hu, M. Khurana, Y. H. Seah, M. Zhang, Z. Guo and D. Zhao, *Chem. Eng. Sci.*, 2015, 124, 61-69.
33. Z. Xiang, X. Peng, X. Cheng, X. Li and D. Cao, *J. Phys. Chem. C*, 2011, 115, 19864-19871.
34. N. H. Alsmail, M. Suyetin, Y. Yan, R. Cabot, C. P. Krap, J. Lü, T. L. Easun, E. Bichoutskaia, W. Lewis, A. J. Blake and M. Schröder, *Chem. Eur. J.*, 2014, 20, 7317-7324.
35. Y. Huang, Z. Lin, H. Fu, F. Wang, M. Shen, X. Wang and R. Cao, *ChemSusChem*, 2014, 7, 2647-2653.
36. Y. Wang, M. He, X. Gao, S. Li, S. Xiong, R. Krishna and Y. He, *ACS Appl. Mater. Interfaces.*, 2018, 10, 20559-20568.
37. Y. Yan, M. Suyetin, E. Bichoutskaia, A. J. Blake, D. R. Allan, S. A. Barnett and M. Schröder, *Chem. Sci.*, 2013, 4, 1731-1736.
38. C. Song, Y. He, B. Li, Y. Ling, H. Wang, Y. Feng, R. Krishna and B. Chen, *Chem. Commun.*, 2014, 50, 12105-12108.
39. F. Chen, Y. Wang, D. Bai, M. He, X. Gao and Y. He, *J. Mater. Chem. A.*, 2018, 6, 3471-3478.
40. Y. Zhang, L. Yang, L. Wang, S. Duttwyler and H. Xing, *Angew. Chem. Int. Ed.*, 2019, 58, 8145-8150.
41. J. D. Humby, O. Benson, G. L. Smith, S. P. Argent, I. da Silva, Y. Cheng, S. Rudić, P. Manuel, M. D. Frogley, G. Cinque, L. K. Saunders, I. J. Vitórica-Yrezábal, G. F. S. Whitehead, T. L. Easun, W. Lewis, A. J. Blake, A. J. Ramirez-Cuesta, S. Yang and M. Schröder, *Chem. Sci.*, 2019, 10, 1098-1106.
42. P. Nugent, V. Rhodus, T. Pham, B. Tudor, K. Forrest, L. Wojtas, B. Space and M. Zaworotko, *Chem. Commun.*, 2013, 49, 1606-1608.
43. S. S. Nagarkar, A. V. Desai and S. K. Ghosh, *Chem. Commun.*, 2014, **50**, 8915-8918.
44. X.-Z. Song, S.-Y. Song, S.-N. Zhao, Z.-M. Hao, M. Zhu, X. Meng, L. L. Wu and H. J. Zhang, *Adv. Funct. Mater.*, 2014, **24**, 4034-4041.
45. S. S. Nagarkar, A. V. Desai, P. Samanta and S. K. Ghosh, *Dalton Trans.*, 2015, **44**, 15175-15180.
23. B. Wang, X. L. Lv, D. Feng, L. H. Xie, J. Zhang, M. Li, Y. Xie, J. R. Li and H. C. Zhou, *J. Am. Chem. Soc.*, 2016, **138**, 6204-6216.
46. B. Q. Song, C. Qin, Y. T. Zhang, X. S. Wu, L. Yang, K. Z. Shao and Z. M. Su, *Dalton Trans.*, 2015, **44**, 18386-18394.
47. S. Mukherjee, A. V. Desai, B. Manna, A. I. Inamdar and S. K. Ghosh, *Cryst. Growth Des.* 2015, **15**, 4627-4634.
48. B. Joarder, V. Desai Aamod, P. Samanta, S. Mukherjee and K. Ghosh Sujit, *Chem. Eur. J.*, 2015, **21**, 965-969.
49. P. Ghosh, K. Saha Sourav, A. Roychowdhury and P. Banerjee, *Eur. J. Inorg. Chem.*, 2015, **17**, 2851-2857.
50. S. Nagarkar Sanjog, B. Joarder, K. Chaudhari Abhijeet, S. Mukherjee and K. Ghosh Sujit, *Angew. Chem. Int. Ed.*, 2013, **125**, 2953-2957.
51. X. Liu, B. Liu, G. Li and Y. Liu, *J. Mater. Chem.A*, 2018, **6**, 17177-17185.
52. R. Fu, S. Hu and X. Wu, *J. Mater. Chem. A*, 2017, **5**, 1952-1956.
53. A. Gogia and S. K. Mandal, *Dalton Trans.* 2019, **48**, 2388-2398.
54. P. Das and S. K. Mandal, *J. Mater. Chem.A*, 2018, **6**, 16246-16256.